FACULDADE DE ENGENHARIA DA UNIVERSIDADE DO PORTO

Metamaterial Antennas for RADAR and SAR

Bruno Filipe Oliveira Correia

Mestrado Integrado em Engenharia Eletrotécnica e de Computadores

Orientador: Sérgio Reis Cunha (PhD)

July 25, 2018

Resumo

Os sistemas de RADAR e Radar de Abertura Sintética (SAR) necessitam de antenas diretivas com banda larga. Para as antenas serem diretivas é necessário que estas sejam grandes, o que é impraticável em muitas aplicações. As antenas com metamateriais são construídas usando estruturas miniaturizadas complexas que permitem que antenas pequenas se comportem como antenas consideravelmente maiores. Esta dissertação propõe um array de antenas miniaturizadas que serão utilizadas em aplicações de RADAR e SAR.

Este trabalho recorre à utilização de metamateriais de forma a existir transformação uma onda polarizada linearmente numa onda polarizada circularmente. Sendo assim, antenas de Vivaldi linearmente polarizadas verticalmente e horizontalmente, irão poder ser utilizadas para emissão e receção simultâneamente, permitindo uso de menores potências de transmissão e o uso de um sinal por um maior período de tempo, evitando portanto a emissão recorrendo a pulsos de elevada potência por curtos instantes temporais. Para além disso, foi desenvolvida e testada uma maneira de tornar o sistema mais compacto e fácil de ser usado em plataformas de teste, usando para isso uma caixa metálica que envolve o array e que serve também de suporte para o metamaterial.

A caracterização do array mostrou que o ganho deste é inferior ao simulado, no entanto foram investigadas e apresentadas possíveis causas para a perda de ganho. No entanto este trabalho é concluído apresentando os motivos pela qual, colmatando as pequenas falhas, este sistema será passível de ser utilizado em sistemas reais de RADAR e SAR.

Abstract

RADAR and Synthetic Aperture Radar (SAR) system require broadband directive antennas. Directivity requires antennas to be large, which turns out to be impracticable in many applications. Metamaterial antennas are built using complex miniaturized structures that produce small antennas that behave equally to much larger traditional antennas. This dissertation proposes a an array of miniaturized antennas that will be used for RADAR and SAR applications.

This work makes use of metamaterials in order to transform a linearly polarized wave into a circularly polarized one. As such, vertically and horizontally polarized Vivaldi antennas can be used for both transmit and receive simultaneously, allowing the use of lower transmission power and the use of a signal of larger temporal duration, thus avoiding the emission using high power pulses for short temporal instants. In addition, a method to obtain a more compact and easy to use on test platforms system has been developed and tested, using a metal box that encloses the array and also serves as a support for the metamaterial.

The characterization of the array showed that the gain of it is inferior to the simulated one, nevertheless, possible causes for the loss of gain were investigated and presented. This work concludes by presenting the reasons why, by filling small defects, this system will be able to be used in real RADAR and SAR systems.

Agradecimentos

Ao meu orientador, Professor Sérgio Reis Cunha, por toda a sua disponibilidade, motivação e, acima de tudo, por todo o conhecimento e aprendizagens que me transmitiu.

À Zaida, por toda a ajuda ao longo do meu percurso académico e pela presença constante na resolução de problemas.

A todos os meus amigos, por todas as lições e experiências que me deram o privilégio de vivenciar. Em especial ao Américo, David e Nuno que desde cedo me ajudaram a traçar um caminho da qual eu estou orgulhoso. Agradeço ao Diogo por todas as opiniões que me deu na elaboração desta tese e por me ter acompanhado em tantas batalhas e ao Rodrigo pelas técnincas de construção mecânicas partilhadas.

À minha família que sempre me apoiou e me deu todas as ferramentas para eu poder traçar o meu caminho. Um especial agradecimento à Marta pela sua presença e por toda a compreensão.

Bruno Correia

"If you want to find the secrets of the universe, think in terms of energy, frequency and vibration."

Nikola Tesla

Contents

List of Figures

List of Tables

Abbreviations and Symbols

ADS	Advanced Design System
AUT	Antenna Under Test
ESA	Electrically Small Antennas
FEUP	Faculty of Engineering of University of Porto
LHCP	Left-Hand Circularly Polarized
PBC	Periodic Boundary Condition
RADAR	Radio Detection And Ranging
RHCP	Righ-Hand Circularly Polarized
SAR	Synthetic Aperture Radar
SNR	Signal-to-Noise Ratio
SRR	Split-Ring Resonator
TSA	Tapered Slot Antenna
UAV	Unmanned Aerial Vehicle
UWB	Ultra Wideband
VNA	Vector Network Analyzer

Chapter 1

Introduction

An antenna is a device that interacts between the waves that propagate in space and the currents that circulate in a metal, which allows transmission or reception of signals. Since the transatlantic transmission achieved by Marconi in 1901, the human being has become increasingly dependent on radio communications. With the quick evolution of the technology and with the best use of the spectrum of frequencies, a greater need for antennas capable of complying with the increasingly more demanding requirements of the systems arise. Smaller and more easily fabricated antennas are now required. They need also to provide less interference with the other components in the vicinity. This work focuses on the miniaturization of antennas and their uses as a set, in a way that they can be used in Radio Detection, Ranging (RADAR) and Synthetic Aperture Radar (SAR).

1.1 Context and Motivation

RADAR and SAR have gained great importance today due to the vast possibilities of use like in the case of oceanography, aerospace and defense. In the specific case of SAR, which has high-resolution capability independent of flight altitude and it is not dependent on weather, it provides a wide range of frequencies to chose from. In order to increase the resolution of SAR systems, there is a need to use antennas with high bandwidth. Furthermore, there is a need for these same antennas to have high directivity, to reach longer distances with the same power. Traditional antennas that would meet the requirements would have to be larger, specially because the performance of the antenna is related with its size, which makes the system harder to implement in airplanes and satellites, where SAR and RADAR systems are mostly installed. So, in RADAR and SAR systems there is a great demand for Electrically Small Antennas (ESA). Additionally, several techniques related to SAR use an array of antenna elements spatially distributed over two dimensions orthogonally to the propagation direction of the electromagnetic waves.

In order to achieve goals that are not physically achievable, materials that have properties not found on nature must be used. These types of structures are called metamaterials. Their precise shape, geometry, size, orientation and arrangement give them their smart properties, capable of

manipulating electromagnetic waves: by blocking, absorbing, enhancing, or bending waves, to achieve benefits that go beyond what is possible with conventional materials.

The desire to contribute to the improvement of existing systems and to an efficient miniaturization led to this dissertation theme. A miniaturized system allows its implementation in Unmanned Aerial Vehicle (UAV) that, being the technology to advance so that they become totally autonomous, can turn out to be the future platforms for the SAR systems.

1.2 Objectives

Several antenna topologies have been used in SAR and RADAR systems. In addition, systems may be used where there are antennas to transmit and separate antennas to receive the scattered signal.

The main objective of this work is to develop a small antenna array based on small Vivaldi antennas. Simulations beginning from the unity cell until an array of antennas are made to meet the established requirements. This allows to model the reference behavior of the array and will allow to characterize the entire system before of the antennas construction. The antenna array should cover a large band passing by L-Band, S-Band and C-Band. In addition, it should be possible to select the operating polarization of the array: vertical, horizontal, right circular and left circular. To add to these requirements, one should make use of and further enhance the inherent directivity of the Vivaldi antenna. It is known that the more antennas in an array, the greater the gain, giving a better SNR and, in addition, more elements in the array reduces the beamwidth, however one of the major challenges of this thesis is to increase the amount of array elements keeping the size reduced as a goal.

In addition, metamaterials are used which allow the transformation of a linear polarization into a circular polarization. In this way, it is possible to use Vivaldi antennas that are cross-polarized without polarization losses.

1.3 Thesis structure

This thesis will be composed by seven chapters. After this one with introductory purposes, the problem that is in the origin of this work will be presented, the approach to solve it, the state of the art and the current state of similar SAR and RADAR antennas systems. It will be an overview of the whole work that will be developed. Chapter 3 will describe the main cell of the system - the Vivaldi Antenna. The various stages until the final design be achieved and the detailed array model of the system will also be shown. Chapter 4 will be devoted to the study of metematerials and their implementation on the system. After the separated subsystems are concluded, the integration and analysis of the entire system will be done in Chapter 5. Chapter 6 concludes, presenting also guidelines for future work

Chapter 2

Overview

This chapter aims at providing the reader with a background of the current SAR and RADAR systems. It will explain how it is used most of the times. Then, it will be presented a systematic overview of the problem and the approach proposed to solve it. This chapter ends with the state of the art which presents developments made in addressed area by other authors and the technology available at this time.

2.1 SAR and RADAR antennas systems

A RADAR transmits a pulse that travels at speed of light and receives some of the energy that is reflected back. A SAR system is a radar system that simulates a large aperture by processing the accumulated scattered signals of a moving antenna, represented in figure 2.1. The amplitude and phase of the backscattered signal depends on the physical (i.e., geometry, roughness) and electrical properties (i.e., permittivity) of the imaged object. [8]

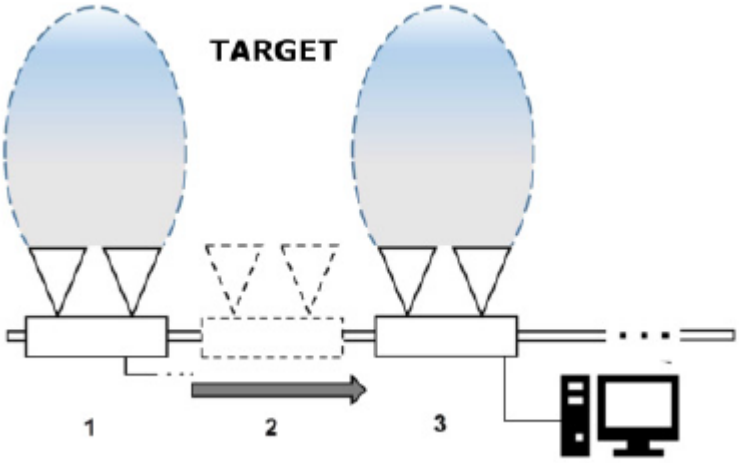

Figure 2.1: Conventional Implementation of a SAR system [1]

The characteristics of the array will be interconnected with azimuth resolution of a SAR system being that, the equation 2.1 represents the length of the synthetic aperture, 2.2 the beamwidth of the synthetic antenna and 2.3 the azimuth resolution. [2]

$$L_{sa} = \Theta_a \times r_0 = \frac{\lambda}{d_a} \times r_0 \tag{2.1}$$

$$\Theta_{sa} = \frac{\lambda}{2 \times L_{sa}} = \frac{d_a}{2 \times r_0} \tag{2.2}$$

$$\delta_a = \Theta_{sa} \times r_0 = \frac{d_a}{2} \tag{2.3}$$

where d_a is the effective length of the array.

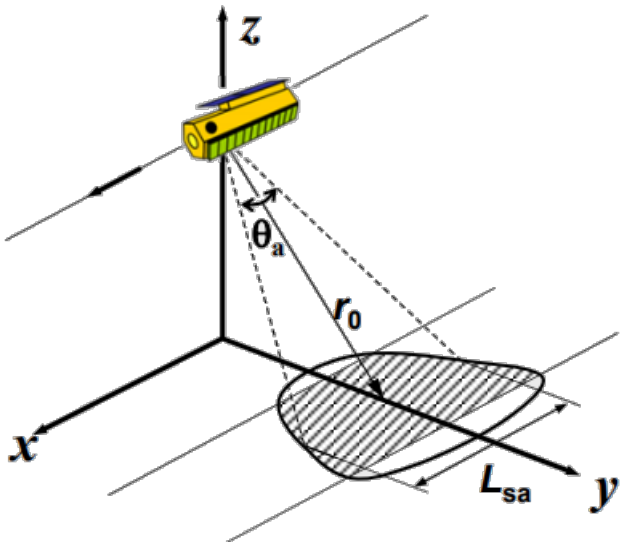

Figure 2.2: Relation between antenna characteristics and SAR resolution [2]

There is a relationship between the gain of the antenna and Θ_{sa}. In fact, the resolution is as large as the effective area of the antennas, so, to reach twice the resolution of a SAR image, it compensates for the use of an array. In addition, using an array allows increasing the gain of the system without causing too large an increase in the effective area of the array. The ideal situation for SAR system is when the array has as many elements as possible, once more elements provides more gain, providing greater SNR. With more elements, it is also reduced the 3-dB beamwidth, providing higher resolution. [9]

2.2 The problem and the approach

Many SAR and RADAR systems use two independent arrays of antennas. One of them is used to transmit and the other to receive the scattered signal. This implies that the assembly of the system

has to be done in a cautious way, since any slight variation in the orientation of the array can cause the loss of a good SNR and thus compromising the system.

The main objective of this thesis is to join the two arrays of antennas in a single one, in a paired way, facilitating the implementation in satellites, airplanes and UAV. In addition, the array will have to be composed of an array as small as possible, in order to minimize the total array size. There are two major problems to overcome with this implementation:

- The crosstalk between the cross-polarized antennas.
- The transmission and reception will be done in the same polarization, however, the transmitting and receiving antennas will be polarized orthogonally, which requires the use of techniques of rotation of the signal electric field.

To solve both problems, a set of metamaterials will be studied. It is also expected that the implementation of these will help to miniaturize the system as well as improve the final array directivity.

The unit cell of the system will be composed by two Vivaldi antennas - one in horizontal position and the other in vertical position as exemplified in figure 2.3 being able to transmit in vertical and horizontal polarizations.

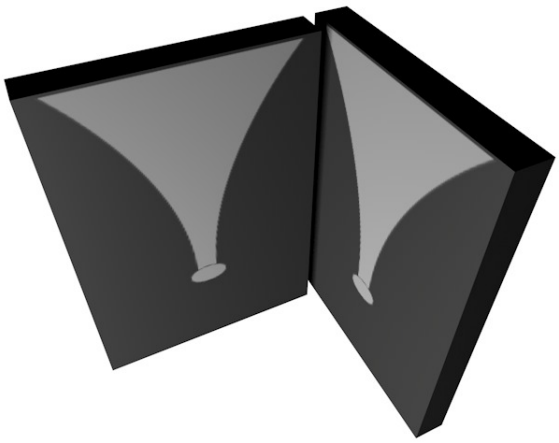

Figure 2.3: Unit cell of the system composed by two Vivaldi antennas in orthogonal position

A problem also to be faced is that the array has to have a good shape shield not to interfere mechanically and electrically with the system around it. As such various materials and possible forms for the support will be studied to hold the Vivaldi antennas and to fasten RF electronics with cables.

2.3 State-of-the-art

Vivaldi antennas will be the focus of this work. Vivaldi antenna, was introduced by Gibson [10] in 1979. Once Vivaldi belong to the Tapered Slot Antenna (TSA) category, it is characterized by its high bandwidth, considerable directivity and gain, and symmetry of the electric field, $\overrightarrow{E}$, and the magnetic field, $\overrightarrow{H}$, radiation pattern.

Vivaldi antennas are low cost, easy to fabricate and fairly insensitive to dimensional tolerances in fabrication process due to printed circuit technology used for the construction of these antennas. Moreover, Vivaldi arrays are small size and low weight enabling compact arrays. [11]

2.3.1 Vivaldi antenna

The proposed Vivaldi antenna consist of a microstrip feed line, microstrip line to slot line transition, and the radiating structure. Radiating structure is exponential tapered and the radiation takes place along the axis of the tapering. On one side of the antenna substrate, an exponential tapered slot is designed starting with a circular slot cavity. The cavity act as an open circuit that minimizes the reflections from microstrip line to slot-line transition [12]. The shape of flaring and cavity determine most of the characteristics of the antenna. To provide feed to the Vivaldi, a microstrip line to slot line transition is designed so that the antenna remains matched over wider frequency band. The microstrip line is designed on the another side of the substrate.

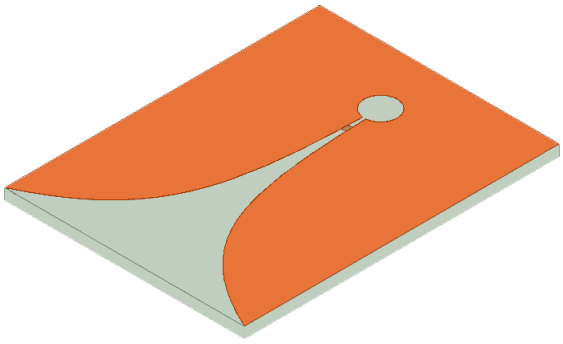

Figure 2.4: Vivaldi antenna

Pandey et al. [12] present the equations that define the tapered profile of the slot:

$$y(x) = \alpha e^{K_a x} \tag{2.4}$$

where constant α and opening rate K_a are given by:

$$\alpha = \frac{s}{2} \tag{2.5}$$

$$K_a = \frac{1}{L_a} ln\left(\frac{W_a}{s}\right) \tag{2.6}$$

where L_a, W_a and s are the aperture length, aperture width and width of slot at origin, respectively.

The Vivaldi antenna is characterized by having a large bandwidth. However, it is necessary to use a feeding technique in order to take full advantage of the antenna. The technique implemented in this work will be stripline to slotline transition. It consists of slots etched on both sides of the substrate and a stripline feeding the slotlines at the center of the substrate. [11]

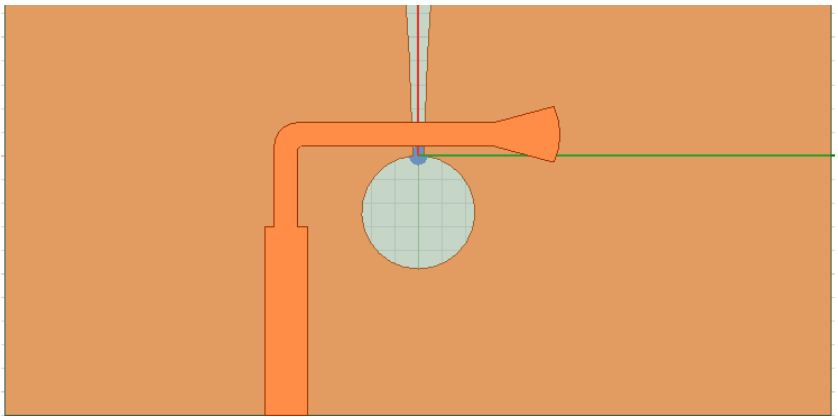

Figure 2.5: Stripline to slotline transition

Regarding the antenna dielectric, it is a FR-4 substrate with relative permittivity of 4.4 with thickness of 1.6mm. This material is abundant and has an affordable price, making the construction of the antennas possible, especially when building an array.

2.3.2 Antennas arrays

Enlarging the dimensions of single elements often leads to more directive characteristics. Another way to enlarge the dimensions of the antenna, without necessarily increasing the size of individual elements, is to form an assembly of radiating elements in an electrical and geometrical configuration. This new antenna, formed by multielements, is referred to as an *array*. [13]

2.3.2.1 Array Pattern

The array pattern can be achieved by the multiplication of a single element pattern and the array factor. The array factor does not depend on the actual element pattern of the array and it is found with the elements of the array replaced with the isotropic radiators.

$$E(total) = [E(\text{single element at reference point})] \times [\text{array factor}] \tag{2.7}$$

It depends on the number of elements used, their spacing, geometrical arrangement, excitation magnitudes and phases.

For N similar element array, the array factor is given by:

$$AF(\Theta) = \sum_{n-1}^{N} e^{j(n-1)\Psi} \tag{2.8}$$

where

$$\Psi = kdsin(\Theta) + \beta \tag{2.9}$$

where β is the difference in phase excitation between elements, d is the distance between elements and k is the wave number.

Array factor can also be described as 2.10 [13], which is a simpler equation and allows to find the nulls, the maximum and the 3-dB of the array.

$$AF = \left[\frac{sin(\frac{N}{2}\psi)}{sin(\frac{1}{2}\psi)}\right] = N \times \frac{sinc\left(N\frac{d}{\lambda}sin(\theta)\right)}{sinc\left(\frac{d}{\lambda}sin(\theta)\right)} \tag{2.10}$$

If we equate the numerator of the equation to zero, we obtain the minimum of the array:

$$sin\left(\frac{N}{2}\psi\right) = 0 \Leftrightarrow \theta = cos^{-1}\left[\frac{\lambda}{2\pi d}(-\beta \pm 2m\pi)\right] \tag{2.11}$$

$$\text{n=1,2,3,...}$$

$$n \neq N, 2N, 3N, ...$$

The array factor has a maximum and it occurs when m=0:

$$\theta_m = cos^{-1}\left(\frac{\lambda\beta}{2\pi d}\right) \tag{2.12}$$

The 3-dB occurs when:

$$\theta_h = cos^{-1}\left[\frac{\lambda}{2\pi d}\left(-\beta \pm \frac{2.782}{N}\right)\right] \tag{2.13}$$

2.3.2.2 Array Configuration

An array can be linear, planar and circular in geometrical arrangement. Linear array is formed by placing the radiators along a line, figure 2.6. The array factor is symmetrical with respect to the line by which the elements are aligned. Nurhayati et al. [14] studied the effect of Vivaldi element antenna from each frequency to the total array pattern and stated that a broadband antenna can have different element pattern in different operating frequency. The linear array is not the ideal for this thesis once it only allows to have the system working in one polarization.

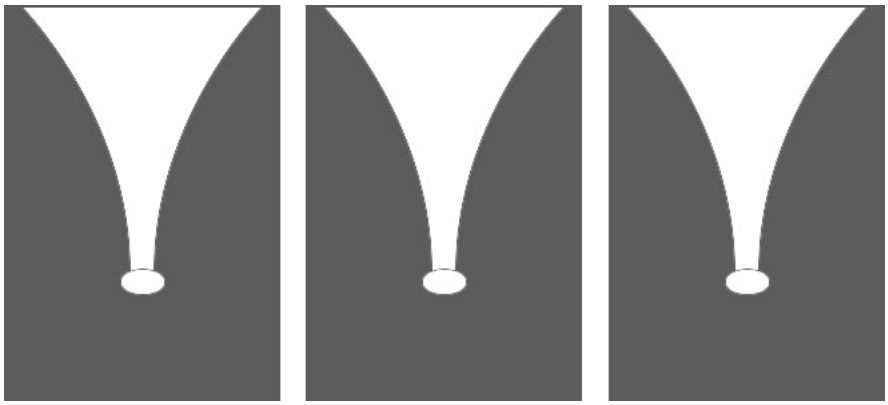

Figure 2.6: Example of a linear array

To form a planar array, in addition to placing elements along a line, individual antennas need to be positioned along a rectangular grid like the example of figure 2.7. Planar array gives the advantage of controlling the radiation pattern and scanning the main beam in the required direction easily and it allows to generate symmetrical patterns with lower sidelobes when compared to those of linear arrays. [11].

Figure 2.7: Example of a planar array

The circular array, in which the antennas are combined in vertical and horizontal position like as shown in figure 2.8. This type of the array is what will be developed throughout this dissertation because it is the scheme that allows a greater diversity of possible polarizations to the system which, in times when the available spectrum begins to be so reduced being necessary to use techniques to take advantage of it, being the optimization of polarizations, one of them. The disadvantage of this type of scheme is due to the low isolation between elements, which leads to greater care being taken in order to avoid resonances affecting the array performance.

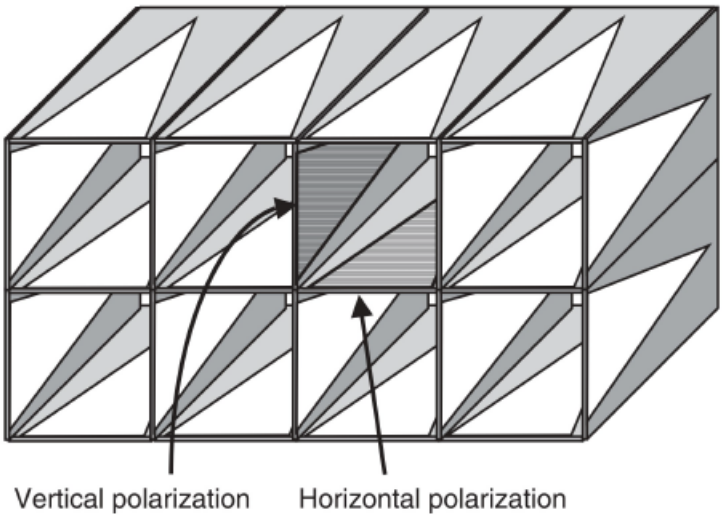

Figure 2.8: Circular array scheme [3]

When constructing an array, the spacing between elements must be taken into account. Grating lobes can be defined as the main beam lobes or maxima in other directions than the desired one. Despite the effect of mutual coupling between the individual antennas increase, in order to avoid grating lobes completely, array spacing should be smaller than one-half wavelength of the maximum operating frequency, $d < \lambda/2$. [11]

2.3.2.3 Array Directivity

The directivity of an antennas represents the ratio between the radiated power that is concentrated in a given direction and the total radiated power. Mathematically representing, one obtains

$$D(\theta,\phi) = \frac{U(\theta,\phi)}{P_{rad}/4\pi} = \frac{4\pi U(\theta,\phi)}{P_{rad}} \tag{2.14}$$

where P_{rad} is the total radiated power. Radiation intensity, $U(\theta,\phi)$, is the power radiated in a given direction per unit solid angle. Directivity can be specified as either a function of direction or as the maximum value. [15]

For tightly coupled array, it is very important to take the mutual coupling between antennas and losses into account, once part of energy radiated by the transmission antennas can be received by the receiving ones affecting the signal quality. The gain of the array varies according to the number of antennas by which it is composed and is defined by equation 2.15

$$G = 10log_{10}(N) \tag{2.15}$$

2.3.2.4 Mutual Coupling

Properties of antenna elements can change dramatically when placed in an array environment. Both the radiation pattern and the input impedance of the elements are altered from free space

values due to mutual coupling. It occurs due to three mechanisms: direct space among array elements, through feed network and indirect caused by near-by scatterers, represented in figure 2.9 as arrow 1, 2 and 3, respectively. [13]

In an array environment the field radiated and scattered by a given element changes the current distributions of the other elements. For an array with Vivaldi antennas, the changes occur in the aperture field distributions. Likewise, the field radiated or scattered by the other elements affects the current distribution or aperture field distribution of the original element. [16]

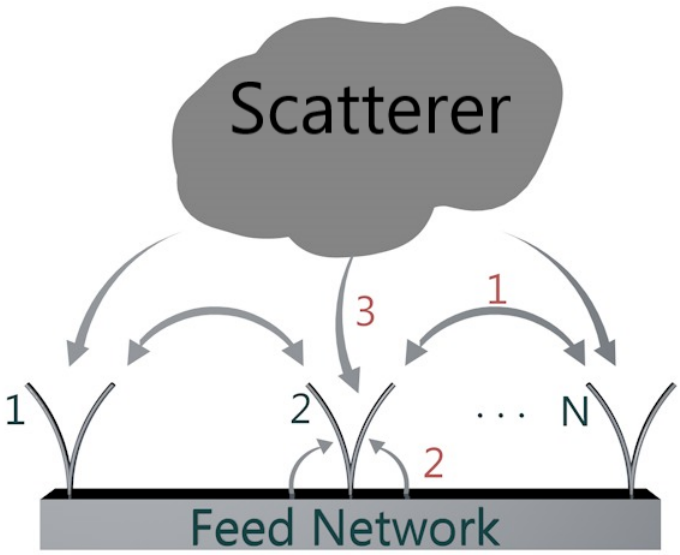

Figure 2.9: Examples of mutual coupling in an array

2.3.3 Polarization diversity

Polarization of an antenna can be seen as the vector that is collinear with the electric field magnitude at a particular point of the far-field. This property can be divided in linear, circular or elliptical polarization. We are facing linear polarization in the case of the vector is always directed along a line. Linearly polarized antennas are the most common because of their simplicity. Vivaldi is a linearly polarized antenna.

In circular and elliptical polarizations, $\overrightarrow{E}$ traces a circle as a function of time. The elliptically polarized field, is a particular case of circular polarization, once it has different magnitudes in two axis. Since the fingers of right hand point in the direction of rotation of the electric field vector when the thumb points in the direction of propagation, this type of wave is referred to as a *right-hand circularly polarized*, RHCP, wave [4]. When the electric field rotates in the opposite direction, it constitutes a *left-hand circularly polarized*, LHCP, wave. The ellipticity of an antenna can be defined by its axial ratio, which is the ratio of the major and minor axis amplitudes. Circular

and linear polarization are special cases of elliptical polarization. An elliptically polarized wave with an axial ratio of 1 is a circularly polarized wave, and an infinite axial ratio for an elliptically polarized wave is a linearly polarized wave.

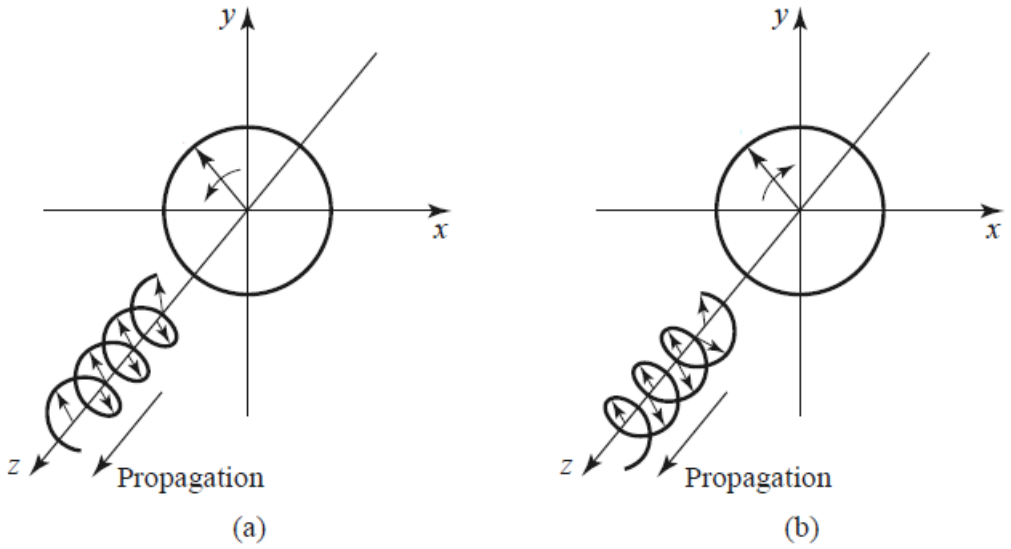

Figure 2.10: Electric field polarization for (a) RHCP and (b) LHCP plane waves. [4]

In order to implement a system with polarization diversity, it is necessary to implement an auxiliary circuit that allows the choice of antennas that will be transmitting the signals and those will be receiving the echoes on the array. It will then be necessary to create a circuit composed of switches. PIN diodes can be used to construct an electronic switching element easily integrated with planar circuitry and capable of high-speed operation, in the order of 20ns if the diode driving circuit is carefully designed. [4]

In [4] it is presented two configurations for the use of PIN diodes:

- Series configuration - the switch is ON when the diode is forward biased.
- Shunt configuration - the switch is ON when the diode is reversed biased.

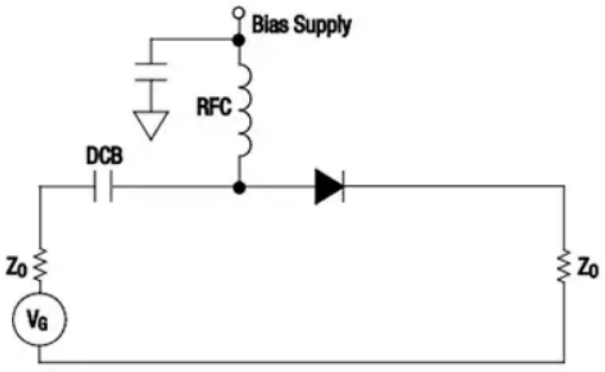

Figure 2.11: Series configuration single-pole, single-throw RF switch [5]

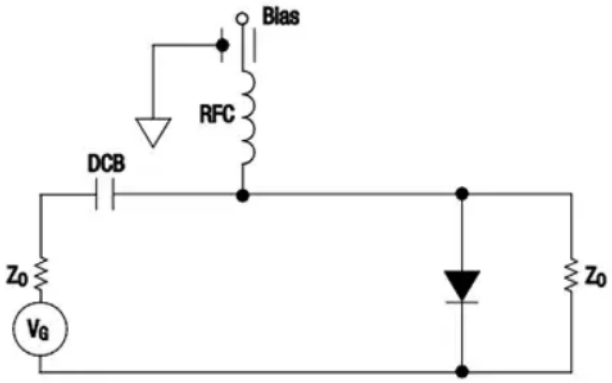

Figure 2.12: Shunt configuration single-pole, single-throw RF switch [5]

Like all electronic devices, these switches do not have an ideal behavior since they have a small attenuation when they are in conduction and do not have infinite attenuation when they are in cut, however some of these non-ideal behaviors can be improved by adding an external reactance in series or in parallel with the diode. [4]

An RF switch is a device that allows switching signals on and off via transmission paths. This allows to change the transmitting and receiving antennas while maintaining the same configuration, eliminating the need for connections and disconnections through the exchange of cables. RF switches are characterized by having a component with approximately -30dB of ratio between an input to the output when the switch is turned off. PIN diodes are the base element of the switches.

2.3.4 Metamaterials

Metamaterial is an arrangement of artificial structural elements designed to achieve advantageous and unusual properties not found in natural materials. [17] They have been designed to a wide range of frequencies from radio up to optical and different functions, like negative refractive index and huge chirality. One of the most important applications of metamaterials is antenna design. Due to their unusual properties, it is possible to achieve antennas with novel characteristics which cannot be realized with traditional materials. [6]

Kumar et al. [18] presented a zero index metamaterial in order to improve the directivity of a Vivaldi antenna.

Michishita [7], as shown in presents a classification of metamaterial antennas as it is applied directly to the antenna or surrounding medium, the type of metamaterial and what can be achieved with the use of this material, as shown in table 2.1.

Another type of property that is interesting and can enhance developments in RADAR area is the fact that there are materials that change the polarization of a signal, such as the chiral medium. The term chiral describes an object, especially a molecule, which has or produces a non-superimposable mirror image of itself. Huge chirality can be designed with metamaterials at arbitrary frequencies, to counteract the fact of in natural materials chirality is usually weak and only at some special frequencies. [6]

Table 2.1: Classification of metamaterials and resulting feature on the antenna [7]

Application	**Type**		**Features**
Antenna element	Resonant	Radiation element	Small
		Parasitic element	Mutual coupling reduction
	Non-resonant		Broadband
Antenna surrounding medium	Electromagnetic bandgap structure		Coupling reduction
	Artificial magnetic conductor		Low-profile
	Negative refractive index lens		Thin and small

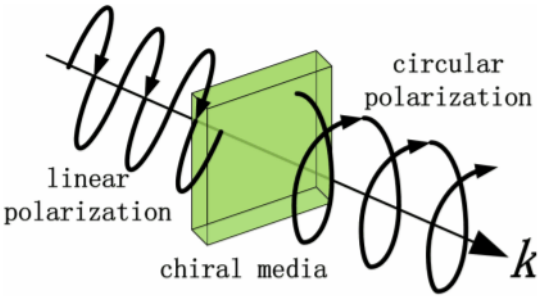

Figure 2.13: The function of chiral media [6]

One of the drawbacks of metamaterials is that they have a narrow bandwidth. However, in order to overcome this problem, it must be clearly ensured that at the frequency of interest the metamaterial is performing a beneficial behavior, otherwise it may be having the opposite effect and not compensating for its use.

Chapter 3

System Overview

The Vivaldi antenna has an end-fire radiation pattern. It offers wide bandwidth characteristics and hence used for wideband signals, also provides a higher directivity than other types of antennas and it can produce a symmetric beam in the $\overrightarrow{E}$ and $\overrightarrow{H}$ planes over a wideband. When used for pulse technologies like RADAR, Vivaldi antennas have a high peak value for the pulse envelope. They offer stable group delay and allow for a narrow pulse width. For these reasons, it is possible to state that it makes this antenna the most suitable for the intended use.

This chapter is split in three subchapters. In the first one, various iterations are presented one by one till the final design is achieved in order to accomplish the desired requirements. The second one, called Unit Cell, is further divided in two sections. The first section details the crosstalk between the antennas and the techniques that were used in order to reduce that phenomenon. The final subsection presents the steps followed for the construction of the array, taking into account mechanical, electrical as well as feeding aspects of the antennas.

3.1 Vivaldi antenna

The implementation of Vivaldi antenna started with the design task, where a printed circuit board (PCB) was designed as a platform for the antenna itself; then, its printing on the PCB corresponds to the first part of the fabrication process. Ansys Electronics Desktop is an unified platform for electromagnetic, circuit and system simulation [19] and it was used to make an accurate characterization of the antenna with respect to S-Parameters, gain and radiation pattern.

In a first stage, based on [12], in order to obtain a reference behavior of a Vivaldi antenna, a first model was simulated.

It is a requirement that the antenna be capable of transmitting and receiving signals at the frequency of 2.3 and 5.3 GHz as such, the first model did not yet cover the range of frequencies desired for this work.

3.1.1 Parametric Analysis

The antenna length should be greater than a free space wavelength at the lowest frequency of operation, 2.3GHz in this case. This requirement assumes a directive beamwidth and a good efficiency for that frequency. However, since in this way one would have an array of dimensions too large for the desired effect, abdicating the value of the gain and beamwidth, an antenna length on the order of the λ_0, where λ_0 represents the desired wavelength at the lowest frequency of the antenna, is also enough to get the desired bandwidth. The wavelength at the center frequency of 2.3GHz is approximately 130 mm.

Antenna width shall be greater than one-half wavelength at the lowest frequency of operation, λ_0, so as to accomplish the desired radiation performance. Decreasing antenna width below this value, decreases the lowest frequency of operation, thus the antenna bandwidth considerably. The antenna width should then be approximately 65 mm.

The tapered design includes choosing the tapered slotline length, the taper rate, and the taper aperture size. These three factors are dependent on the length and width of the antenna. First, the tapered slotline: it shall be in the order of a λ_0 in order to get the desired gain and beamwidth performance. The bandwidth is also increasing with an increase in the taper length. The taper rate also has a significant effect on the S_{11} parameter of the antenna. Decreasing it improves mid-band response effectively while the low band performance is deteriorated. Thus, the lowest frequency of operation is increased decreasing bandwidth. Furthermore, beamwidth is also dependent on the taper opening rate, since the larger the aperture, the higher the antenna's sidelobes. About the taper aperture size: the radiation of the waves propagating through the slotline increases with increasing slot width further from the half-wavelength of the operating frequency, λ_0. Thus, the aperture shall be on the order of one-half wavelength at the lowest frequency, at least, in order to improve radiation efficiency through the antenna.

Considering the values that were presented as the minimum sizes for the antennas parameters, it is verified that the dimensions of the antenna, and consequently the array, would be too large for the desired effect. However, by making several simulations and after verifying the existence of a resonance in the antenna around the frequency of 2.3GHz, it was decided to make use of this factor and to increase the lower edge operating frequency of the antenna. Thus, it was aimed to not have such a wide antenna bandwidth and to tune the oscillation observed around the 2.3GHz. In this way, it was possible to reduce the length and width of the antenna.

As mentioned in subsection 2.3.1, the proposed Vivaldi antenna also consists of a microstrip feed line and microstrip line to slot line transition. In this case, the main objective was to achieve a feed consistent with the broadband that Vivaldi offers, so it was decided to use radial stubs. In addition it was necessary to ensure that the antenna was matched to 50 Ω because the interface with the system would be through a 50 Ω SMA connector. The characteristic impedance of microstrip line is given by equation 3.1.

$$Z_0 = \frac{120\pi}{\sqrt{\varepsilon_{eff}}[W/d + 1.393 + 0.667ln(W/d + 1.44)]} \tag{3.1}$$

where ε_{eff} represents the effective dielectric constant:

$$\varepsilon_{eff} = \frac{\varepsilon_r + 1}{2} + \frac{\varepsilon_r - 1}{2} \frac{1}{\sqrt{1 + 12d/W}} \tag{3.2}$$

The slotline width varies in accordance with the stub's longitudinal dislocation in the antenna's axis, where it coincides with the feed microstrip line. If the slotline width changes, its impedance would change too and it would affect the conveyance of the slotline to the microstrip line. It would alter antenna's impedance, and consequently the impedance matching and S_{11} parameters.

Radial stubs were the best option to increase the bandwidth and reduce overlapping between the microstrip and slotline, then several possible angles were tested in order to optimize the reflection coefficient of the antenna. Since radial stub angle value alteration does not entail a significative variation for the low and high cutoff frequency values, optimization methodology can be availed through the simultaneous evaluation with the other factors of the line that feeds the antenna.

The use of the cavity offers the freedom to tune the impedance matching, and this affects the bandwidth of the Vivaldi antenna. Increasing the radius of the cavity slot results in lower reflection coefficient value, so, the minimum beamwidth can be obtained for a larger radius of the cavity.

Figure 3.1 represents a scheme for the Vivaldi antenna. For the front and back part of Vivaldi, the green layer of the model is the substrate, FR4 held along PCB. The orange layer is made of copper – in order to enable the electrical conduction.

The final, already optimized, measurements for the antenna are shown in table 3.1 and its variables are represented in figure 3.1.

Table 3.1: Antenna measurements

Parameter	Dimension (mm)
L	55
W	35
Lt	35
s	0.29
d	4.8
L1	8
L2	3.4
L3	1.3
W1	1.8
W2	1
W3	1
Ang	90 deg
radius_s	2.8
lm_dis	11

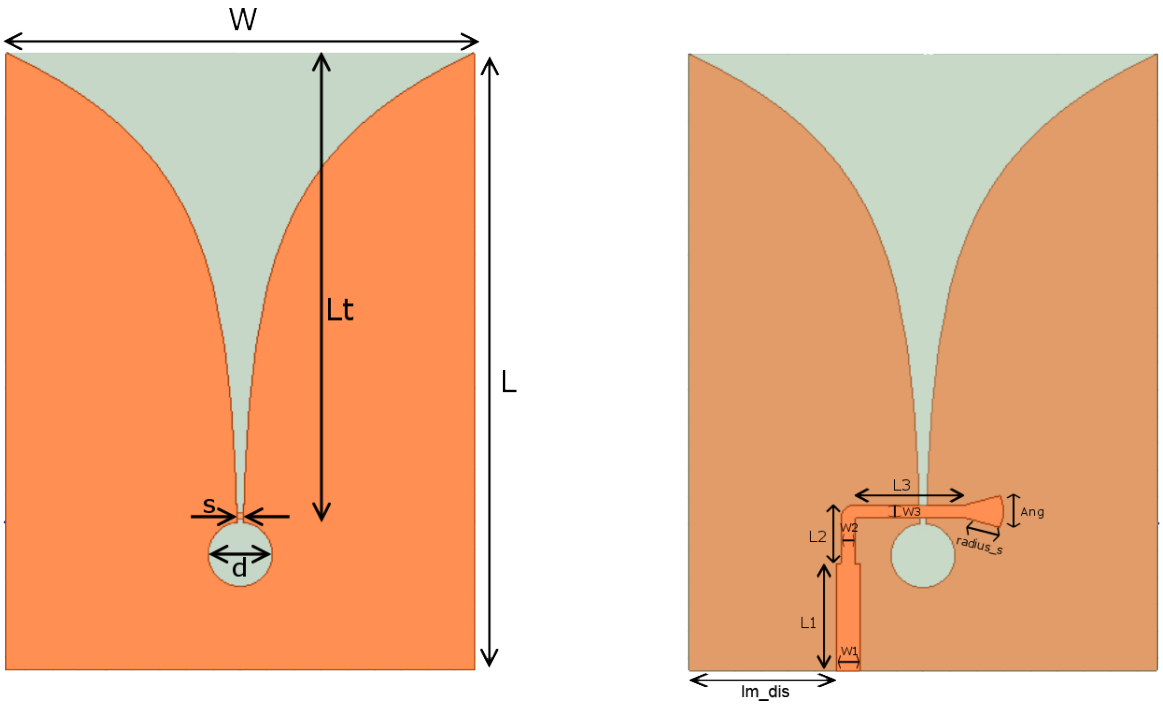

Figure 3.1: Vivaldi model as a whole: front and back sides of the designed PCB

The results of the antenna simulation with the measurements presented in table 3.1 are shown in figure 3.2.

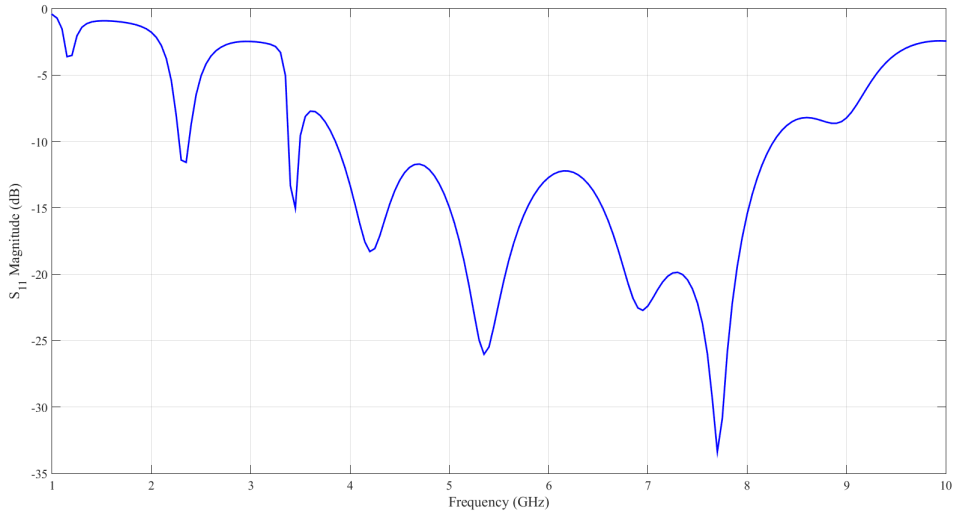

Figure 3.2: S_{11} parameter for the Vivaldi antenna

A system requirement is for the antenna to operate, in addition to the C-Band, at 2.3 GHz. It is then verified that the antenna already fulfills the necessary frequency range. It was also made a

more detailed study of antenna behavior for the RADAR and SAR frequencies at gain level.

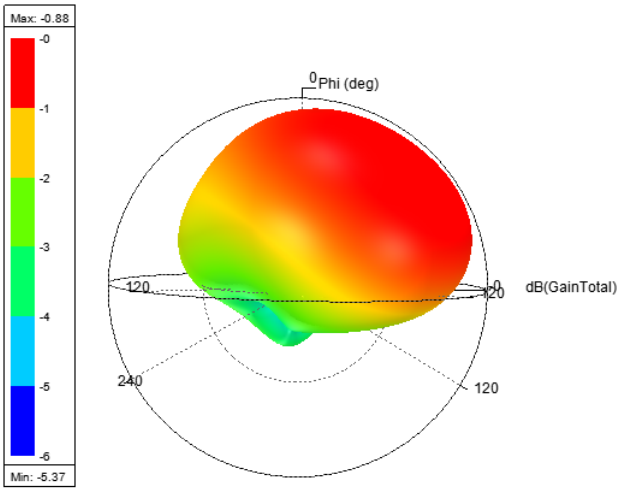

Figure 3.3: Three-dimensional plot of radiation pattern for 2.3GHz

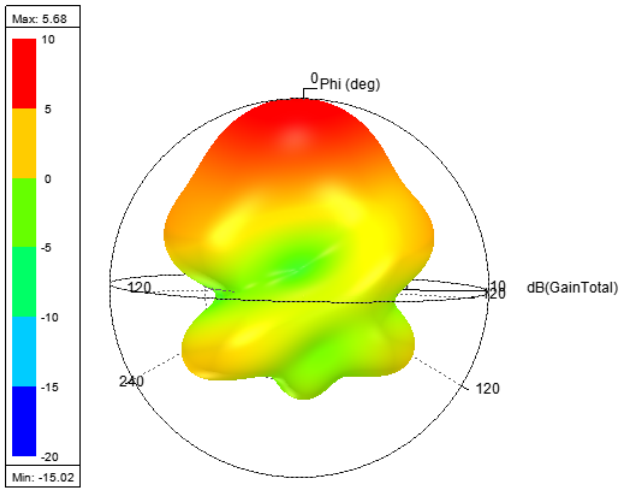

Figure 3.4: Three-dimensional plot of radiation pattern for 5.3GHz

By analyzing the radiation pattern for both frequencies it is found that the antenna is radiating in boresight direction, as desired. However, for the 2.3GHz frequency the gain value is not the desired one once is less than 2dB. As for the radiation pattern of 5.3GHz, this has a value of approximately 5.7dB which, for an antenna with a smaller size when compared to the expected sizes, is an admissible value for this purpose.

3.1.2 Corrugations

Although the bandwidth already covers the range of the proposed frequencies, the gain of the antenna had to be improved mainly in the 2.3GHz frequency. In order to identify the possible problem, a behavioral analysis of the antenna was made with regard to the distribution of currents on its surface. In figure 3.5 it is represented the current distribution of the antenna.

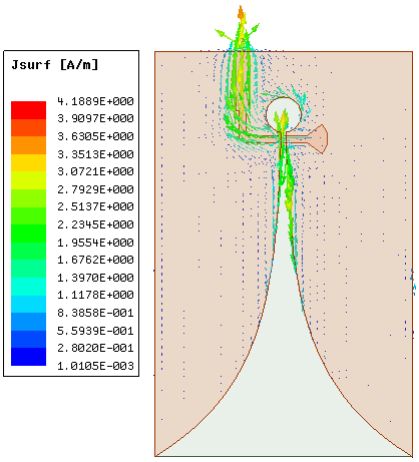

Figure 3.5: Current distribution of the normal Vivaldi antenna at 2.3GHz

The maximum radiation from the Vivaldi antenna should be along the axis of the exponential tapered slot which is due to maximum surface current distribution along the inner edges of the tapered slot. But in practice, the surface current is not only concentrated toward the inner edges but also toward the outer edges of the metallic flares [12]. The surface current on the outer edges of the slot causes side lobe and back lobe radiation, which reduces the radiation of the antenna in boresight direction, which is why the gain is reduced at 2.3 GHz. Therefore, to concentrate the maximum surface current towards the inner edge of the slot, an array of slots of different lengths, also referred as corrugations, is etched from the outer edges. The corrugation acts as a high impedance region forcing the maximum currents to remain near the ends of the exponential surface towards the inner edge of the tapered slot. [12]. In figure 3.6, it is represented the current distribution for the corrugated Vivaldi antenna.

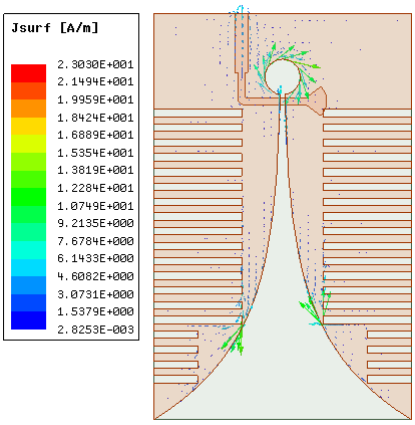

Figure 3.6: Current distribution of the corrugated Vivaldi antenna at 2.3GHz

By analyzing the figure, it is easily proven that the corrugations are creating the expected effect on the currents' distribution. The improved surface current near the inner edge of the slot results in a maximum radiation in boresight direction with reduced side and back lobe radiation. In order to assess the impact that corrugations make on the gain, the polar diagram of the gain for to 2.3GHz are represented on figures 3.7 and 3.8 .

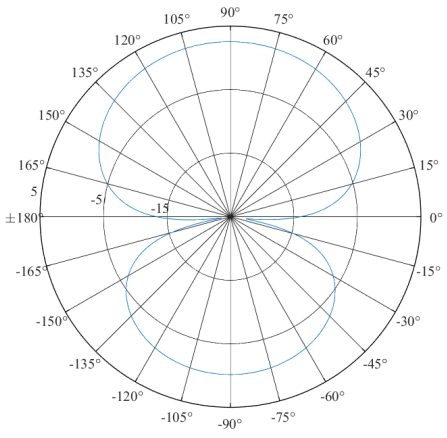

Figure 3.7: Radiation pattern of the corrugated Vivaldi antenna for 2.3GHz

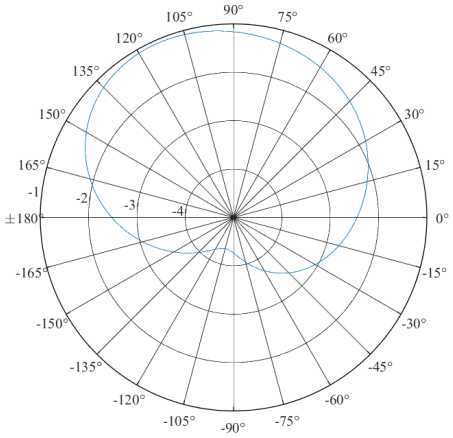

Figure 3.8: Radiation pattern of the normal Vivaldi antenna for 2.3GHz

Looking at the radiation pattern of each Vivaldi antenna configuration, one can easily understand the differences in direction and magnitude of the radiation pattern; that is, for Vivaldi with corrugations, the direction of the radiation pattern has a back lobe, however, the highest concentration of electric field is propagating in the boresight direction, causing the gain to reach a maximum value of 3dB. For the normal Vivaldi antenna, as expected, the gain is smaller since the electric field is spread in the direction of propagation so that its maximum value reaches only approximately -1dB. Comparing the magnitude of both configurations, it is possible to verify that there is

a difference of 4dB. Actually, that means two and a half times more energy when comparing the corrugated Vivaldi antenna with the normal one.

For the 5.3GHz frequency, the current distribution is shown in figures 3.9 and 3.10 for antennas with corrugation and without corrugation, respectively.

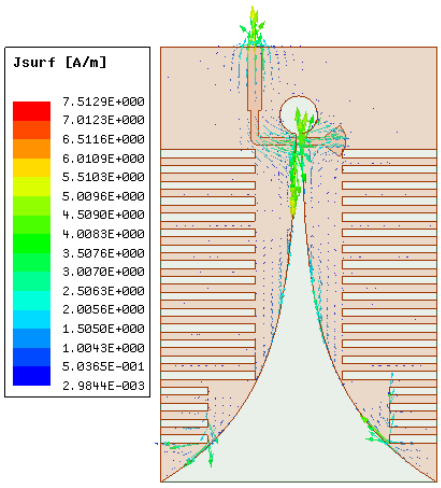

Figure 3.9: Current distribution for a corrugated Vivaldi antenna

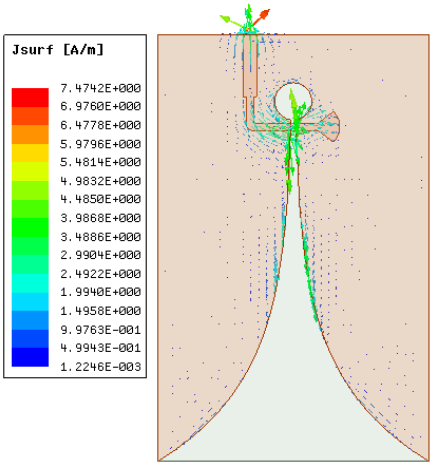

Figure 3.10: Current distribution for a normal Vivaldi antenna

It is verified that for a frequency of operation of 5.3GHz the antenna behaves similarly with and without corrugations. However, even then, it is possible to verify that at the extremities of the Vivaldi with corrugations, more currents circulate in the most extreme zone of the antenna, again improving the direction of propagation of the electric field. Figures 3.11 and 3.12 represent the radiation pattern for each corrugated and normal Vivaldi antenna, respectively.

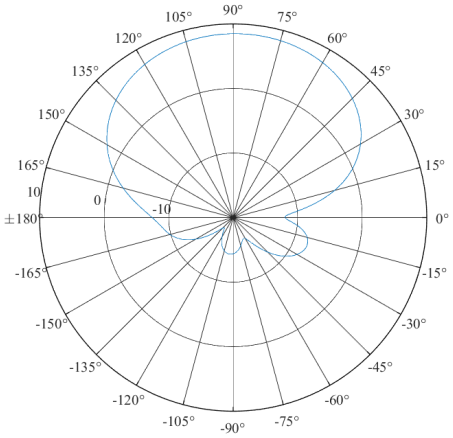

Figure 3.11: Radiation pattern of the corrugated Vivaldi antenna for 5.3GHz

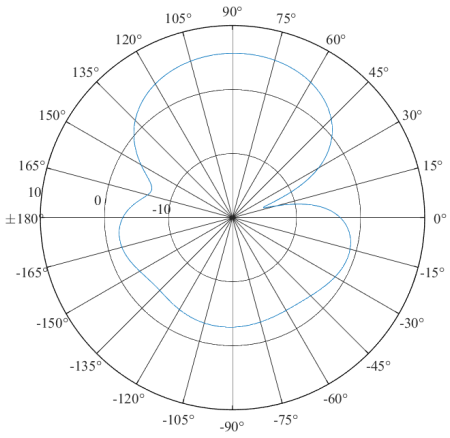

Figure 3.12: Radiation pattern of the normal Vivaldi antenna for 5.3GHz

By doing a detailed analysis of the radiation pattern of both configurations at 5.3GHz, it is again verified that the behavior of the antenna with corrugations has the most directive electric field when compared to the normal configuration. For the corrugated case, the gain reaches 8.5dB, while in the normal case only 5.5dB is achieved, which represents two times the energy.

The fact that the antenna is more directive is due to the fact that it contains lower side lobes which makes the coupling between the antennas in the array smaller throughout its frequency range.

In addition, the slots force the currents to travel a larger path, which is equivalent to creating an inductance. Increasing the inductance also increases the quality factor and, as such, the antenna bandwidth would also increase. It is then concluded that due to the corrugations, the lower edge operating frequency of the antenna also reduces which adds to the antenna miniaturization. It was the fact that the antenna was miniaturized, that at the frequency of 2.3GHz the gain improvement was also evident.

Due to the clear improvements presented in the case of the corrugated antenna, it is possible to conclude that this configuration should be the chosen one for the array.

3.2 Unit cell

As stated in subchapter 2.2, the unit cell of the system is composed by two Vivaldi antennas - one in a horizontal position and the other in vertical position. The main objective of unit cell simulation is to study the small-scale behavior of the system since a two-port system is faster to simulate computationally. Thus, by determining the position of the antennas between them, only the process has to be replicated until the whole system is reached.

In order to study the best positioning for antennas to have the least possible coupling between them, several simulations were performed, where only the positioning of the horizontal antenna in relation to the vertical was changed. In addition, a study was also made of the distance that the antennas would have to be between each other in order to optimize the main beam of the system. Having in possession all the values, the relative position of the antennas, as well as the distance between them, was decided, starting to the array's simulation.

In addition to the electrical study of the system, the analysis of the unit cell also allows designing possible designs to structure the array mechanically. This is a challenging task as the antennas have to be equally spaced from each other, and in addition, have to form a sufficiently rigid structure to be subjected to tests under conditions which may contain vibrations.

3.2.1 Simulation of the unit cell at position 1

In this position, the antennas are orthogonal to each other and are arranged as shown in figure 3.13.

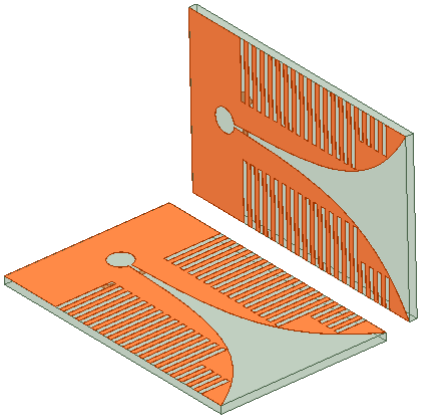

Figure 3.13: Unit cell disposition at position 1

In figure 3.14 are represented the S-Parameters of the unit cell of the system when is implemented at position 1. The parameter S_{21} is the equivalent of verifying which attenuation one antenna has when the other is transmitting.

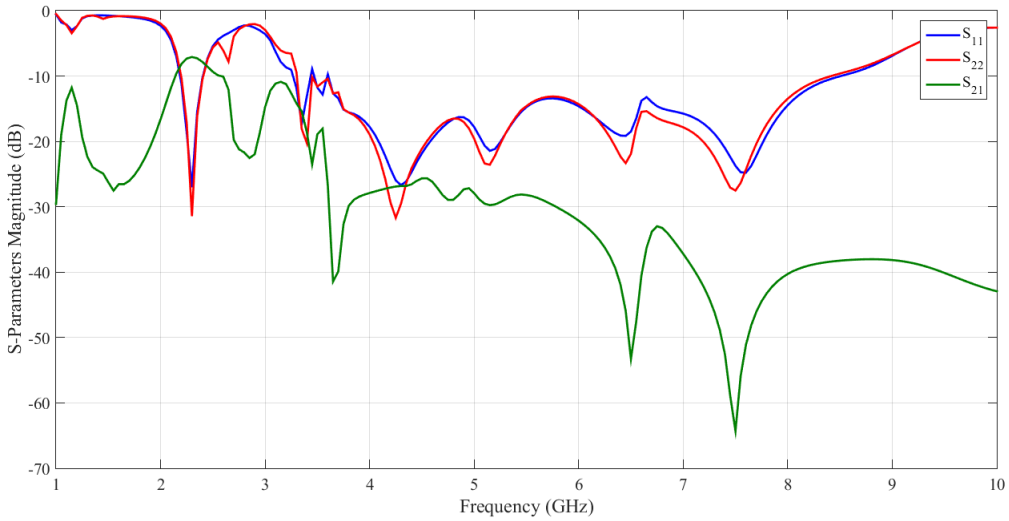

Figure 3.14: S-Parameters of the unit cell at position 1

From the presented data, it is possible to conclude that there is a large coupling between the two antennas at the frequency of 2.3 GHz which makes it difficult to use the systems. However, for the 5.3GHz frequency it is possible to verify an attenuation in the order of 30dB which exceeds the requirement that the antennas must have an attenuation of 20dB between them. The high coupling that exists in the 2.3GHz frequency is due to the fact that the antennas are radiating in a way not as directive as expected, causing the energy to dissipate to the sides, interfering with the other antenna.

3.2.2 Simulation of the unit cell at position 2

The unit cell in position 2 is similar to the above. The difference is due to the fact that the antenna that is horizontal is in an upper zone with respect to the antenna that is in the vertical, whereas in the previous case the reverse happens, as can be seen from figure 3.15.

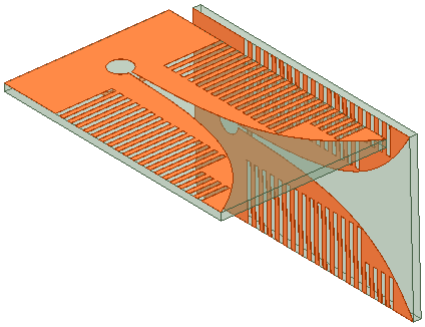

Figure 3.15: Unit cell disposition at position 2

In figure 3.14 are represented the S-Parameters of the unit cell of the system when is implemented at position 2.

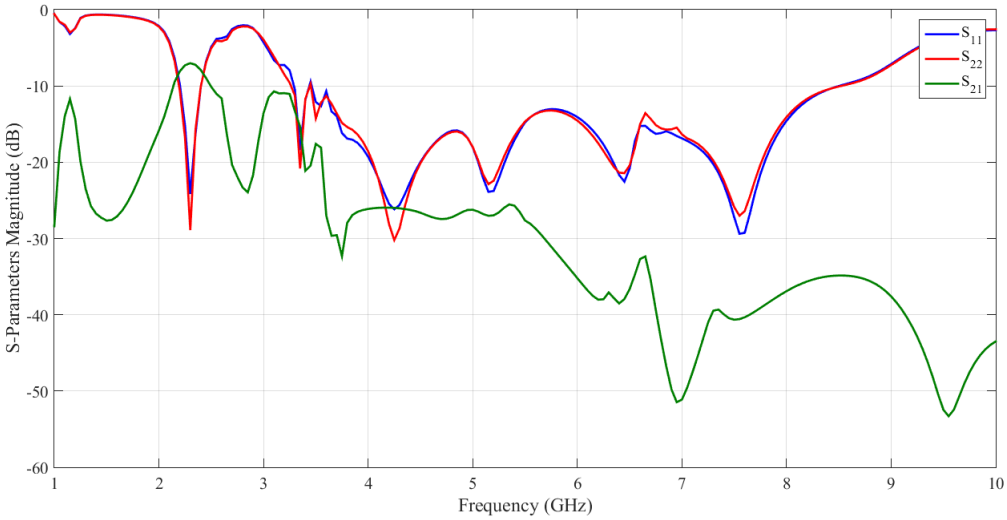

Figure 3.16: S-Parameters of the unit cell at position 2

As expected, since the Vivaldi antenna has a radiation pattern and a symmetrical current distribution, the result was similar to that of position 1.

3.2.3 Simulation of the unit cell at position 3

In position 3, the two antennas remain in an orthogonal position, but the difference is that the antenna in the horizontal position is placed along the center of the vertical antenna and not in one of the borders, as in the two previous cases. Figure 3.17 represents the 3D model of the unit cell at position 3.

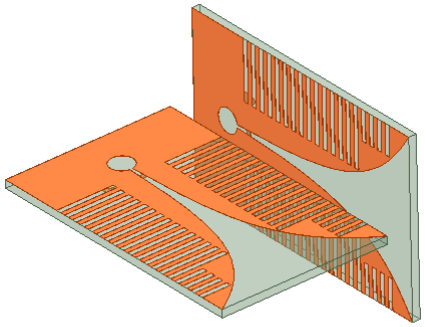

Figure 3.17: Unit cell disposition at position 3

Finally, the simulated S-Parameters for the unit cell at position 3 is given by figure 3.18.

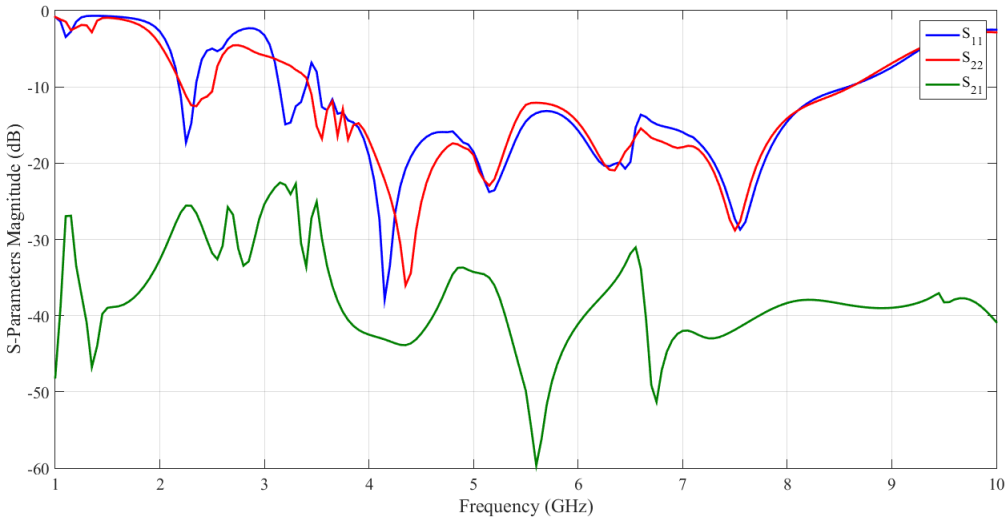

Figure 3.18: S-Parameters of the unit cell at position 3

In this last simulation, it is possible to verify that the coupling of the antennas decreases considerably, mainly in the frequency of 2.3GHz. This is again due to the fact that the antennas have part of their electric field and consequent energy coming out of the antenna's extremities. Placing the horizontal antenna in the center of the vertical is preventing antennas from picking up the electric field from each other. In addition, in the center, since there is no metal in the central

zone of the antenna, there are no currents to circulate and in the same zone, the antenna directs all its energy forward.

In addition, simulations were made where the change was made in the fact that the antenna rotates 180^{o} on itself, which causes only an inversion of antenna layers. As can be seen in figure 3.20, the variation that is present in the S-Parameters of the antennas is negligible, which allows concluding that the rotation of the antenna on itself is irrelevant, as expected.

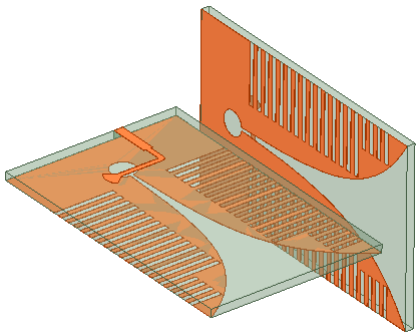

Figure 3.19: Unit cell disposition at position 3 with horizontal antenna rotation

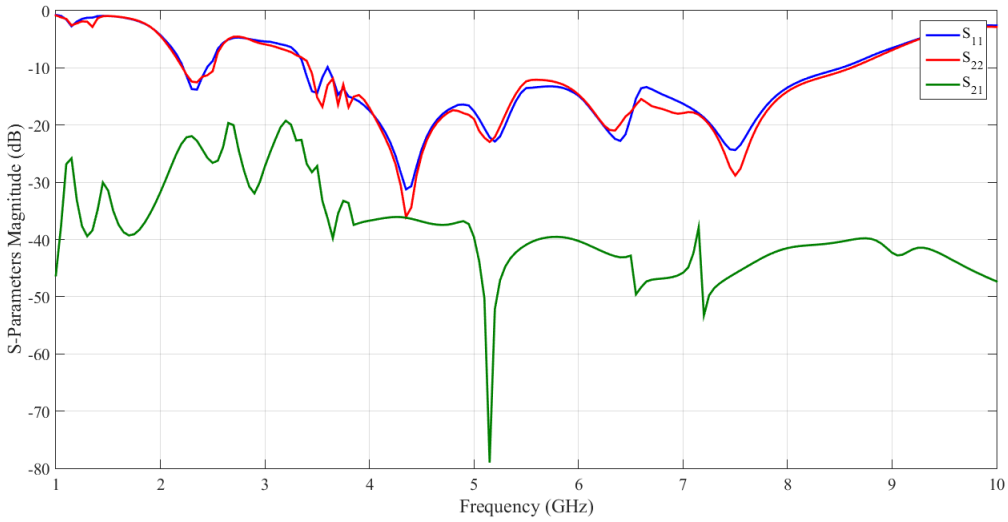

Figure 3.20: S-Parameters of the unit cell at position 3 with horizontal antenna rotation

In addition to the relative positioning of the antennas, the unit cell was also used to study the distance in which the antennas had to be between each other. A minimum spacing of 1mm was considered in order to be able to construct the array without the aid of automatic mechanical equipment and a maximum spacing of 10mm so that the array remains as compact as possible. After simulations for all intervals, it was considered that the ideal distance between antennas

should be 5mm. With this value, parameter S_{21} met the requirements of -20dB and mechanically the array would be compact.

Once the unit cell simulations have been completed, it is possible to conclude that the best option is to place the horizontal antenna in a central position with respect to the vertical antenna, being the position of the layers irrelevant to the coupling factor and to the radiation pattern. Only antennas were tested in these positions because then, in the construction of the array, the system would be balanced. Otherwise, if the horizontal antenna were not in the center or at one end of the vertical antenna, the system would have a much higher construction requirement and could generate asymmetries in the radiation beam.

3.3 Array

Since a unit cell antenna configuration now exists, it makes sense to proceed to an analysis of the array itself, whose final objective is to determine the array's characteristics, in order to obtain the desired directive radiation pattern. Having said that, throughout this subchapter, issues related to the analysis and design of this array are discussed.

As it was mentioned before in this thesis, this array of Vivaldi antennas was built to be integrated into RADAR and SAR systems. Due to the small size of satellites, UAVs or even aircraft that can support SAR systems, the array structure must be compact and take up as little space as possible. As such, it is necessary to take into account two factors: the distance between the antennas, a subject already discussed in section 3.2 and, finally, the mechanical structure of the array together with the PCB that contains the power dividers.

The array consists of 32 antennas in total, 16 horizontal and 16 vertical. Throughout this subchapter will be presented the electrical studies together with the mechanical necessities that are associated with the construction of the array, in the sense of studying the best way to construct the array without this implying interference between antennas.

The proposed solution for the construction of the array went through the assembly of eight sets of equal dimensions, where each one contained four equally spaced antennas in a single plate. Four sets are applied on the horizontally placed antennas and the other four for the vertical case, being that the difference between the two sub-arrays was in the cut that was made for the fit between arrays. Figure 3.21 shows an example of a set of four antennas.

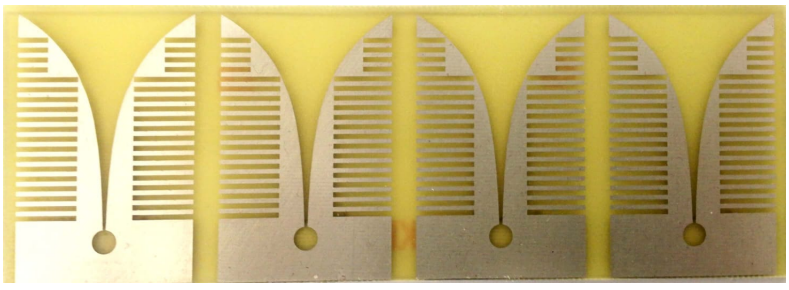

Figure 3.21: Set of four antennas

The results of the S-Parameters of this set of antennas are shown in figure 3.22.

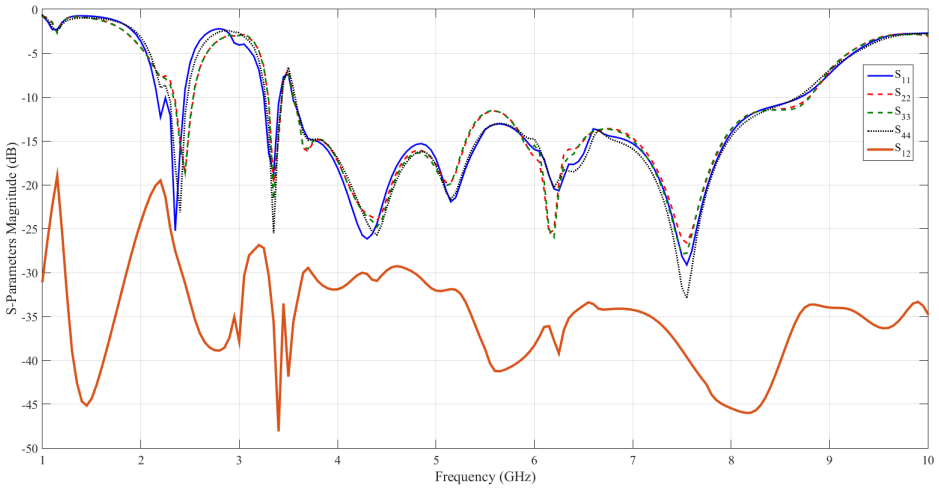

Figure 3.22: S-Parameters for the set of four antennas

By analyzing the S-Parameters of the antennas it is possible to verify that they all have a similar reflection coefficient, as expected. In addition, this same reflection coefficient is comparable to that of the antenna individually, because the antennas are not interfering with each other. In addition, using parameter S_{21} as an example, it is found that the antennas continue with a coupling factor which meets the requirements of the system.

The decision to manufacture the antennas in sets of four comes with the fact that the FR4 that exists between antennas can be used to construct sockets between the antennas. In this way, the horizontal antennas have a specific cut in their plates and the same happens for the vertical antennas only with a different cut. With this method, it is possible to maintain a compact and lightweight system without this implying a total weight increase. Figure 3.23 shows the cuts made on the vertical and horizontal antennas, respectively from top to bottom.

Figure 3.23: Fitting cutouts for the antennas.

The shape of the cut in the antennas allows a robust fit between them. In addition, glue was used in the grooves to secure and strengthen the system. Figures 3.24 and 3.25 show how the antennas fit together and the HFSS model used to simulate this effect.

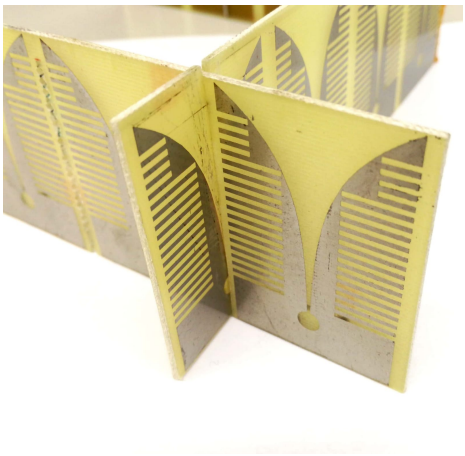

Figure 3.24: Fitting between antennas

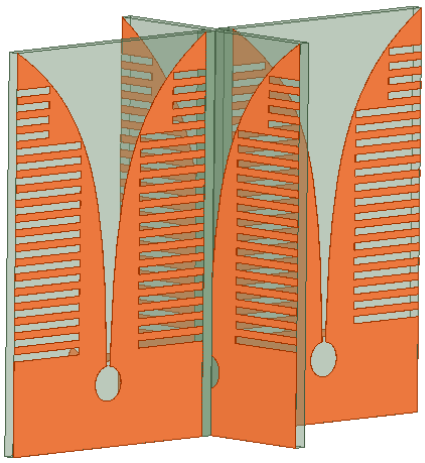

Figure 3.25: HFSS model for the fit between antennas simulation

In figure 3.26 the S-Parameters of the antennas are represented in the arrangement in which they were constructed.

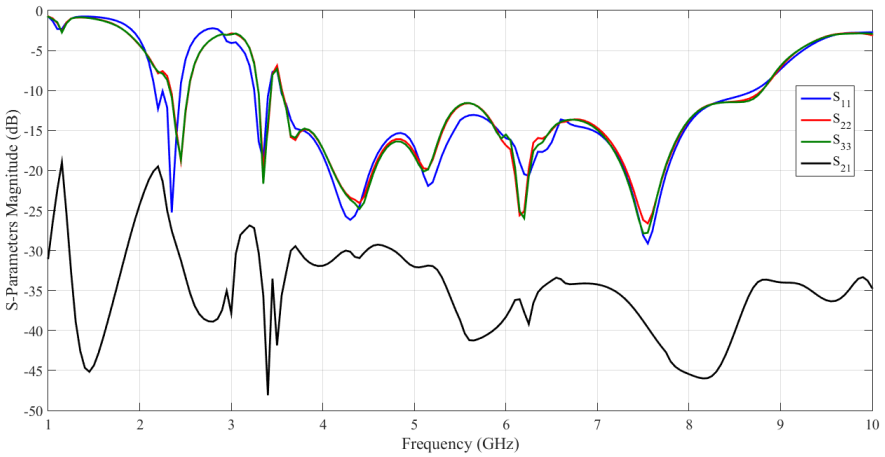

Figure 3.26: S-Parameters for the proposed mechanical arrangement for the antennas

Analyzing the results, it is verified that the technique implemented for the mechanical construction of the system does not interfere with the reflection coefficient of each antenna, as well as keeping the coupling factor between antennas reduced, as desired. The low interferences are due to the above-mentioned effects of the Vivaldi antennas radiate in the boresight direction and, in addition, the currents are circulating in the zone of the exponential and not in the extremities, near of the other antennas. It can, therefore, be concluded that this method of assembling and constructing the antennas does not create interference in an order of magnitude that is detrimental

to the system since each antenna in the array is operating in a similar way to that which would operate individually in terms of the magnitude of S-Parameters.

The process was repeated for the remaining antennas, securing them in the same manner. In figure 3.27 it is possible to verify the final state of the array with the antennas in their final positions.

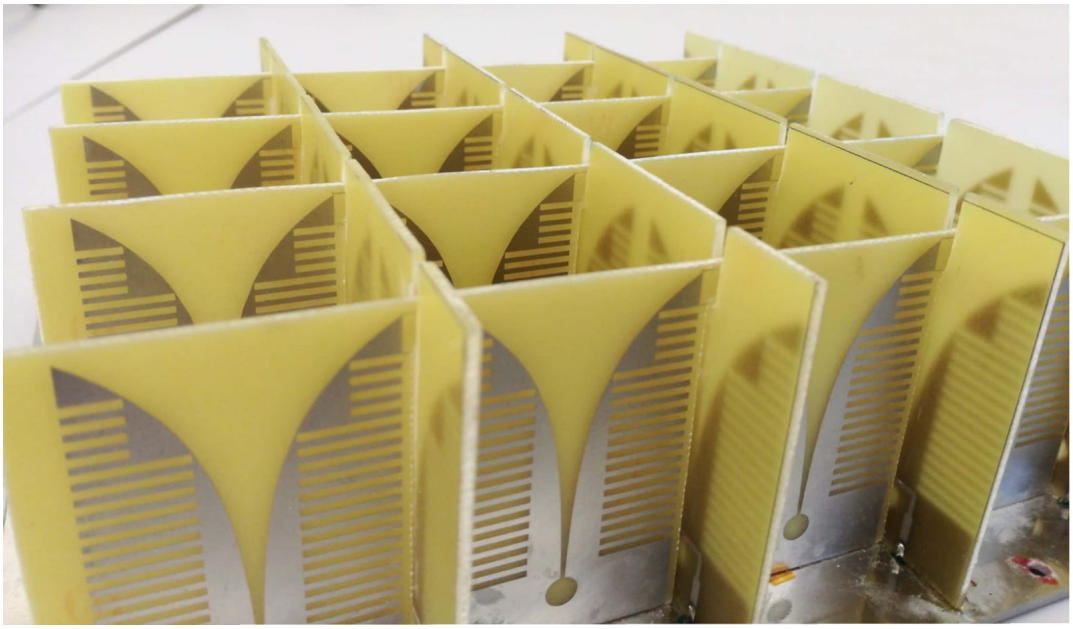

Figure 3.27: Proposed mechanical arrangement for the antennas

In addition to the robustness achieved, it is possible to highlight that, with this method, it is possible to place the antennas in a position extremely orthogonal to each other which makes the system extremely equivalent to the one simulated, which makes the real system reliable and with some results close to those that were simulated.

As for the array, it was also simulated using the HFSS software. However, it was only possible to simulate a maximum of ten antennas for the system since above this value the computer could not simulate due to lack of memory. The solution then went on to design the unit cell of the system composed of two antennas, each one of them in the orthogonal positions, and then use an HFSS tool to calculate the gain of the array based on its array factor. The problem that arises from this simulation is that it does not take into account the mutual coupling between the antennas, nor does it consider the effects of the antennas in the extremities to behave differently from those in the central position. However, given the simulations performed and the positive results, it was considered that this form of simulation would serve as a feasible approximation. To perform this simulation, it is necessary to specify the number of cells along the X and Y axis and how close they are to each other. After this, HFSS presents the expected final result for the array radiation pattern for 2.3GHz and 5.3GHz, as shown in figures 3.28 and 3.29, respectively.

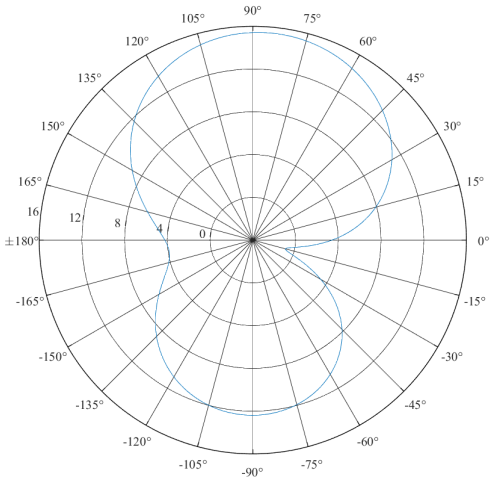

Figure 3.28: Simulated radiation pattern for the array at 2.3GHz

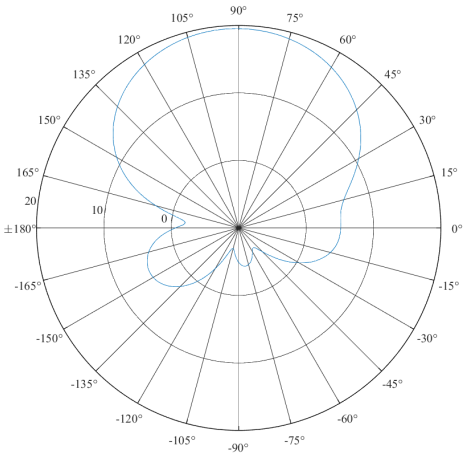

Figure 3.29: Simulated radiation pattern for the array at 5.3GHz

As expected and since the gain of the antenna at 2.3GHz is less than the gain at 5.3GHz, so does the total gain of the simulated array. As seen in the radiation patterns the maximum gain at 2.3GHz is approximately 15.5 dB, while the 5.3GHz is 19.6 dB. The simulated values for the gain of an array of 32 antennas in which their size is reduced to the frequency at which they operate are very satisfactory for the purpose of this thesis.

3.3.1 Power dividers

Since the array was composed of two distinct chains, one for transmitting and one for receiving, two sets of one-to-sixteen power splitters were initially designed and then built. The design phase consisted of two stages: the drawing part of the schematic and the layout section. In both steps, the S-parameters of the antennas were inserted in order to know if the result of the system was the one that complied with the requirements. The simulations were made using Advanced Design System (ADS), which is an electronic design automation software for RF, microwave, and high speed digital applications [20], that was used to design and simulate the RF network of the system for the feeding of the Vivaldi antennas.

In subsection 3.2, the distance at which the antennas should be spaced apart, 5 mm, was found. As such, the distance between each antenna feed should be 40 mm, with each antenna being 35 mm wide. It was with this requirement that one then proceeded to design the power dividers.

3.3.1.1 Schematic design

The first step in the power dividers simulation was to distribute the power dividers by several layers, since each set of 1:16 power divider would have to stay on different layers with a ground layer between them for no EM interference between them, caused by the currents that circulate in the substrate. In addition, it was necessary to have a top and bottom layer of ground, so as to connect the ground of the antennas with the power dividers and the SMA connector, respectively.

In total, the PCB would have five layers, however, the manufacturer would only accept six, which led to having two layers of GND separating the power layers. A stripline consists of a central conductor surrounded by dielectric material between two groundplanes. With equation 3.3 the line width was calculated for an impedance of 50Ω and 25Ω.

$$\frac{W}{b} = \frac{30\pi}{\sqrt{\varepsilon_r} Z_0} - 0.441 \tag{3.3}$$

where W is the strip width and b is the total height of the substrate.

As for the design of the power dividers, one started by joining the antennas in sets of two, and from there join all the sets until there is only one single point of connection that interfaces with the receiving/transmitting equipment. Figure 3.30 represents the junction between two antennas. This is initially composed by the S-parameters of the antennas exported from the HFSS simulation. After that, lines with the 50Ω impedance connect directly to the antennas, then join to a junction transmission line. That 25Ω line from the parallel of the two 50Ω transmission lines connects to a tapered that smoothly makes the transition of an impedance line of 25Ω to 50Ω.

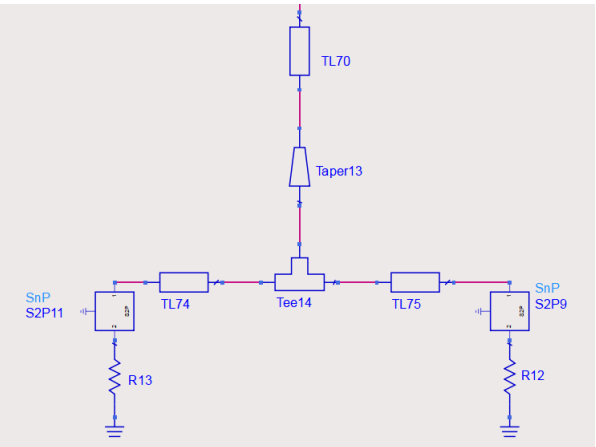

Figure 3.30: Schematic representative of the union between two antennas.

The process repeats itself for all sets of antennas. In figure 3.31, it is possible to examine the procedure of joining two sets of antennas and verify that it is similar to what happens with the junction of the antennas.

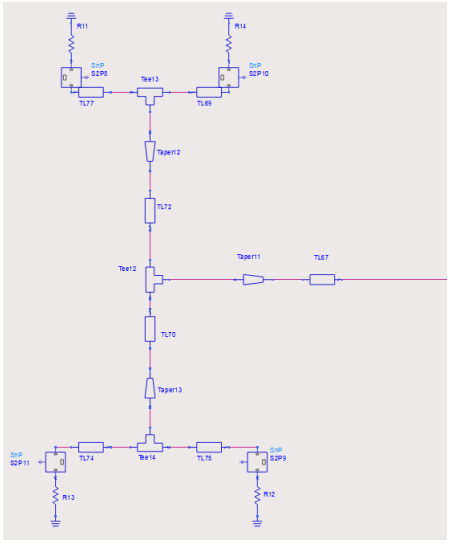

Figure 3.31: Schematic representative of the union between four antennas.

The final result for one set of the power divider is then represented in figure 3.32.

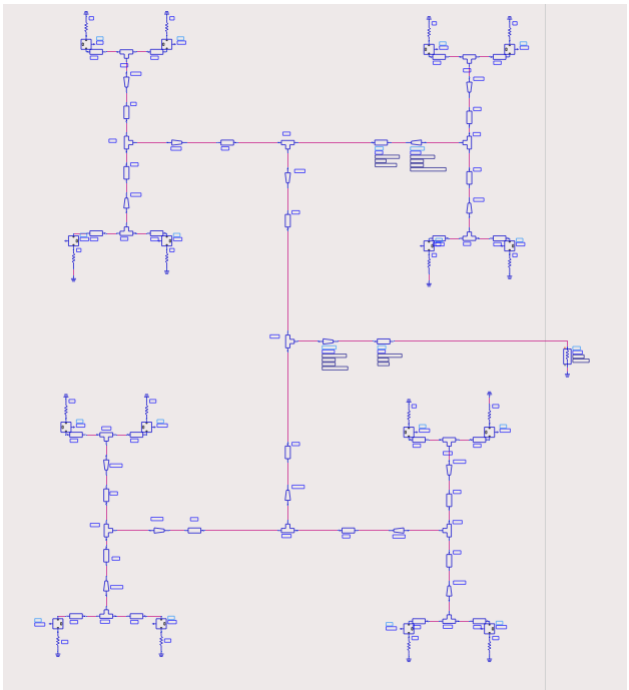

Figure 3.32: Schematic representative of one set of power dividers.

During project development, variables were assigned to the lengths of the lines to ensure that they would be the same length as each other. In addition to ensuring that the antennas would be well spaced apart, it was necessary that all lines would have the same lengths so that no differential phase delays were introduced in the lines. If there is a phase difference between the antennas, the direction of the radiation pattern changes and it is not in boresight direction anymore.

The total height of the substrate of the PCB to be constructed is of 1.6 mm. Since each power divider works separately of the other one and it is designed in half of the PCB, 0.8 mm was used to simulate the schematic height of just one of the power dividers.

The tunning tool of ADS was used to tune the values of the lengths of the striplines and the radius of the corners to achieve the desired result.The final result was reached for the schematic simulation, shown in figure 3.33.

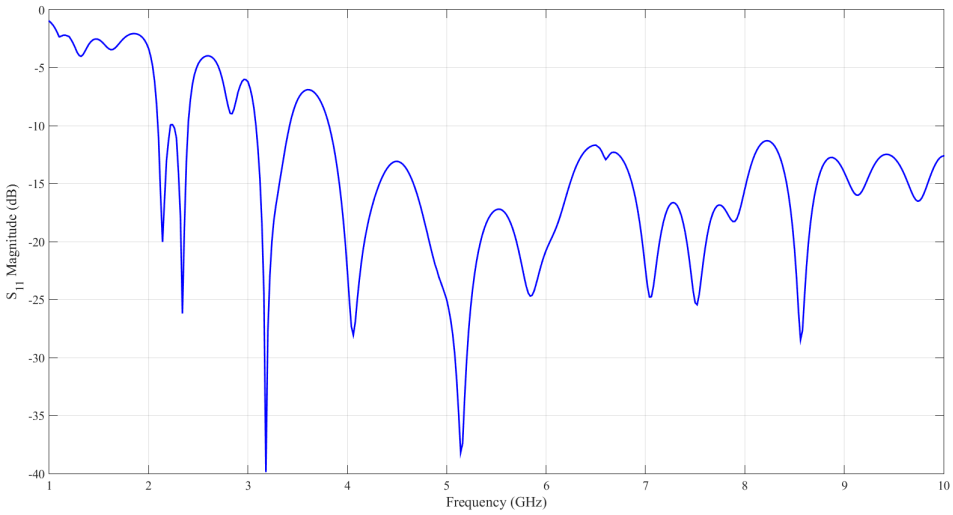

Figure 3.33: S_{11} parameter from the schematic simulation

From the results of the simulation, it is possible to verify that at the 2.3GHz and 5.3GHz the reflection coefficient continues to be below -10dB, which meets the system requirements.

3.3.1.2 EM simulation

Before the layout design and simulation, the substrate of the system was defined so that the correct layers were assigned to the different systems. Figure 3.34 represents the distribution of the layers in the substrate.

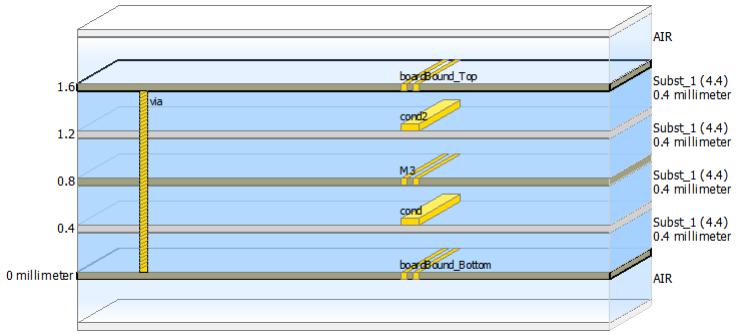

Figure 3.34: Layer distribution on PCB substrate

The substrate is then composed of four layers of FR4 with a relative dielectric permittivity of 4.4. The bottom layer is composed of a layer of copper of 35 micrometers in its part of the bottom, ”boardBound_Bottom”, and by the power divider in its part superior, ”cond” layer. The second layer has no copper underneath and has a copper layer on top, ”M3”, while the third layer has a copper layer underneath, ”M3”, and the second power divider on its top, ”cond2”. The fourth and last layer has no copper on its bottom, however, it has copper on its top, ”boardBound_Top”. It is also possible to verify that the type of routes to be used, through hole technology, is present in the substrate. This type of lanes is simpler to implement for a manufacturer and as such, the total cost of the PCB is lower when compared to the use of blind vias. The difference in this type of vias is that in the first type, it crosses the entire substrate of the PCB, making a connection from the top to the bottom and, from that, creating contact at all the metal points it crosses. For the blinds, the layers have to be drilled separately, assembled, and then the holes are plated by only connecting a certain layer to the top or bottom of the PCB.

For layout design, ADS tool that allows to generate the layout from schematic was used, resulting in the design shown in figure 3.35.

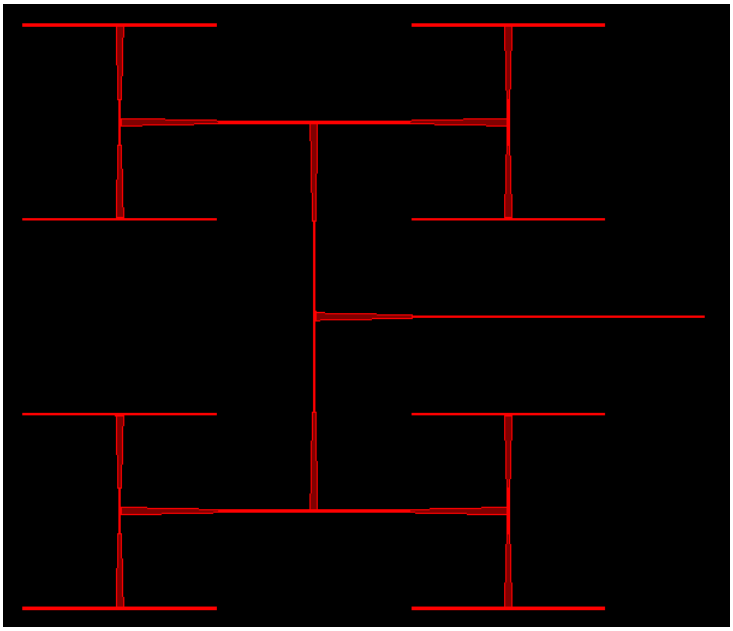

Figure 3.35: 1:16 Power divider layout

Both power dividers are equal to each other, as previously refereed. However, attention had to be paid once again to the distance between antennas being coincident with the calculated value by HFSS. It was also necessary to make sure that the point where they were to be fed would not interfere with the power dividers of the other set of antennas, since, as mentioned above, metallic through-hole vias would be used to feed the antennas using welding cables of the same size to connect the antennas to the PCB. The second power divider is then translated 26.5 mm in the horizontal axis and -5 mm on the vertical axis. Figure 3.36 represents the two power dividers. The fact that they are in two different colors is representative of being in two distinct layers, the

red one, ”cond” layer, connecting to the vertical antennas and, in blue, ”cond2”, connects to the horizontal antennas.

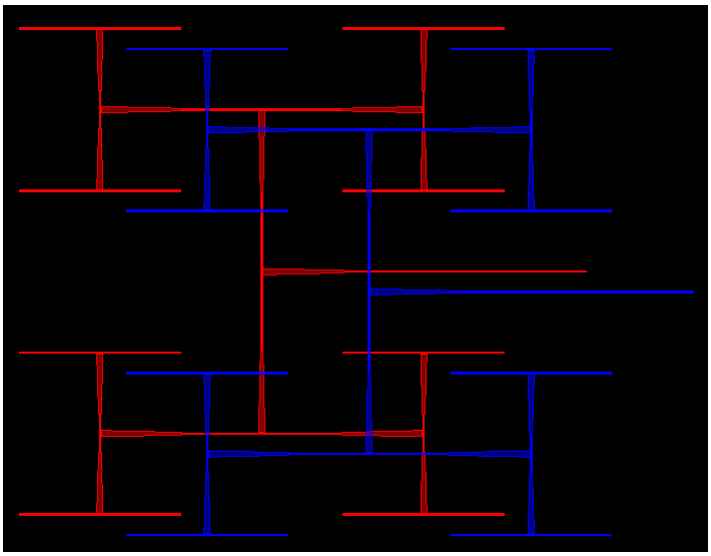

Figure 3.36: 1:32 Power divider layout

After the power dividers were drawn, one moved to the stage of laying the vias, along with the upper and lower ground planes of the board. An empty space between the pads and the rest of the plate was left to prevent short circuits. In the two intermediate ground planes that serve to reduce interference due to the crosstalk of both power dividers, this extra space was also taken into account in order to avoid the contact between the ground plane and the signal. Finally, vias were used to connect the four layers of ground and, thus, it is possible to have a circulation of the currents, also reducing the interferences. The final design of the PCB is then shown in figure 3.37.

Following the designed was finalized, the electromagnetic simulation of the system was started. This type of simulations uses a solver that allows obtaining the S-parameters, allowing to have a model for any passive structure that is correctly defined. It solves the mesh or grid pattern of cells either in the X direction or in the Y direction, so it can do very well coupling simulations. In addition, it takes into account the effect that the intermediate copper plates and the top and bottom have on the layers that have the power dividers, being that at the end of the simulation is expected that the final result is very similar to the fabricated PCB.

In order to obtain faster simulation results, the range of frequencies to be simulated was reduced, while maintaining the frequencies that were a requirement for the system. Figure 3.38 represents the data obtained from the EM simulation to the PCB that contained the power dividers taking into account the S-Parameters of the antennas in their inputs.

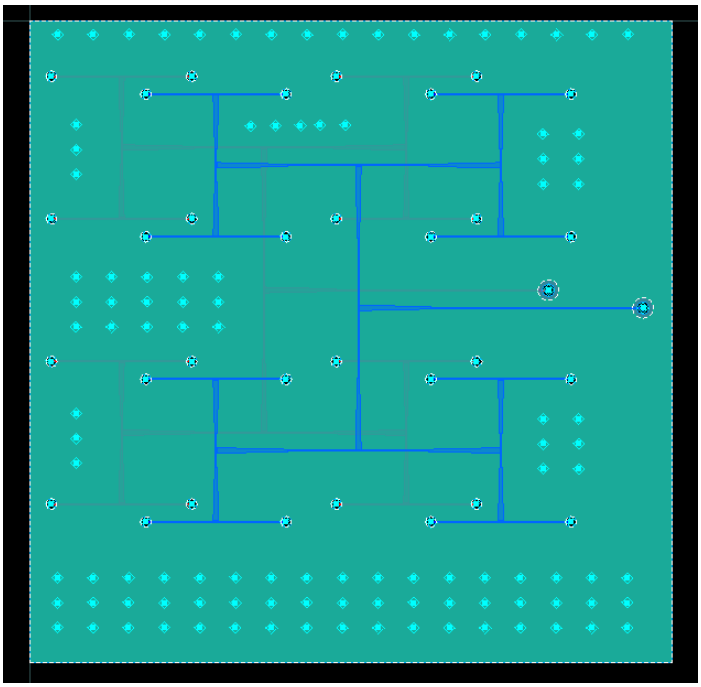

Figure 3.37: Complete design for the power dividers PCB

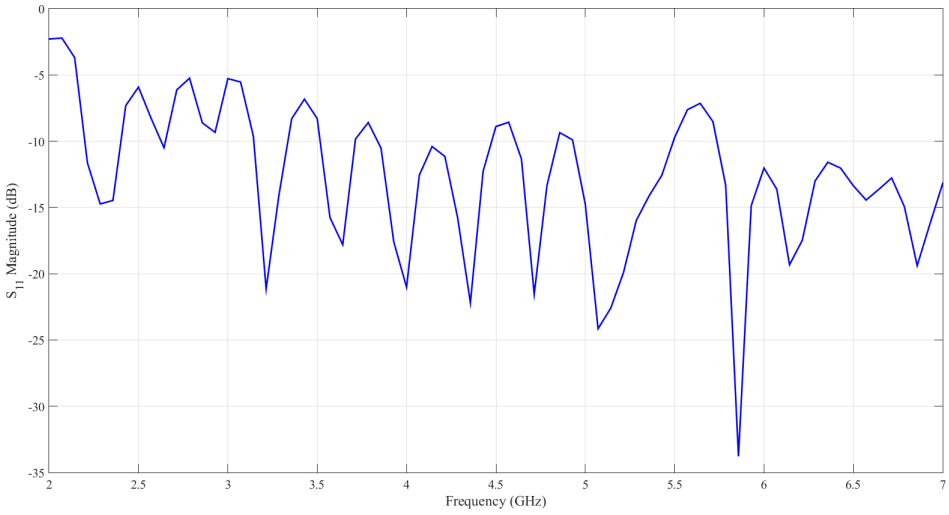

Figure 3.38: S_{11} parameter from the electromagnetic simulation

From the results of the simulation, it is possible to verify that there are ranges of frequencies where the S_{11} is higher than -10dB, making the antenna efficiency lower at these frequencies, however, they are not used. In addition, it is possible to observe that in the ranges of interest of the antennas support signals with a bandwidth above 100 MHz when centered in the 2.3 GHz and 5.3 GHz. Even with good isolation separating power dividers and having vias that allow the circulation of currents, the system is always affected.

An analysis was made to quantify losses associated with substrate and PCB lines. For this, a

simulation was done where a power of 0 dBm was injected at the output of the signal and it was verified how much of it arrived at each port that would connect to an antenna. After the simulation was performed, an arithmetic mean was obtained between the power values reaching all ports and reached the value of $3,747 \times 10^{-5}$ W, which corresponds to -14.263 dBm. Discounting 12 dB derived from the four power divisions along the path, it is easily concluded that the substrate losses are 2.263 dB for each path, meaning that each antenna will decrease this value at its gain.

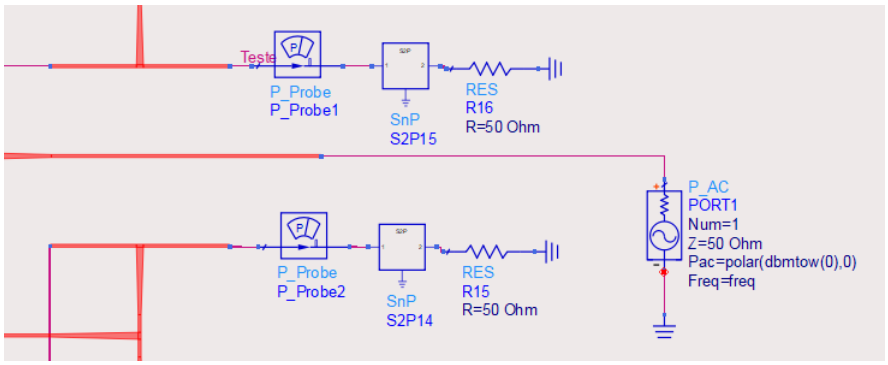

Figure 3.39: Simulation of losses in the substrate and lines focusing on 2 ports

One way to achieve a better result and reduce the range of values to exceed -10 dB and not have so many losses, would be to use a ceramic substrate, that would have fewer losses and have a better frequency behavior at high frequencies. However, as already mentioned in this thesis, the FR4 is a material that is cheaper, which allows the large-scale replication of these PCBs, making the system cheaper.

Chapter 4

Metamaterial

It is known that when a signal is transmitted in horizontal polarization, its echo is received in the same polarization and the same happens for the vertical case. However, when a signal is emitted in right circular polarization, its echo is received in left circular, being reciprocal for the left circular case. Since Vivaldi antenna is linearly polarized, a polarizer based on a chiral medium which has the capability to transform a linearly polarized wave into a circularly wave was placed in an end-fire position making possible the simultaneous transmission and reception in the array. There are also metamaterials that allow improving bandwidth or gain of Vivaldi, however, these materials would have to be placed in an end-fire position of the antenna on the same plate, which would cause the total size of the antenna to be increased and would make the system lose some of its robustness. In addition, the metamaterials are known to present losses, as such, the system would present many losses when joining several metamaterials, thus losing efficiency.

4.1 Slot ring resonator

A Chiral property changes the polarization of an incident electromagnetic wave. In natural materials, chirality is usually weak and only at some special frequencies. However, huge chirality can be designed with metamaterials at arbitrary frequencies.

A linear polarization transformer based on twisted Split-Ring Resonator (SRR), a symmetric chiral metamaterial, was used. A SRR consists of a pair of concentric loops etched in a dielectric substrate with splits in them at opposite ends. These loops are made of a nonmagnetic metal.

The bottom SRR is rotated 90° with respect to the top one. When the structure is illuminated by a normally incident linearly polarized wave, the two linear components of the transmitted wave have nearly equal amplitudes and 90° phase difference around the resonant frequency.

When a time changing magnetic field penetrates through the metallic rings, it induces an electromotive force by Faraday's Law of electromagnetic induction, which in turn produces a rotating current. The ring produces its own magnetic field which may enhance or oppose the incident field. In these structures, the strong chirality is caused by the coupling between the twisted structures on the different layers, without a direct metallic connection.

In each SRR, two modes are possible. One of them is the dipole mode, which occurs when the excitation is along the direction of the connection of the two gaps. The presence of the gaps has no direct effect on this mode, since it does not interrupt the current flow. Also, this mode does not show a resonance since no excitation will be made through the metamaterial in order to exploit this mode. The other mode is the "gapped" loop current mode. This occurs when the excitation is along the direction normal to the metamaterial. The gapped mode is thus only possible thanks to the presence of the gaps [6].

A split ring can be represented by an equivalent *LC* circuit as given in figure 4.1. The capacitance part comes because of the split in the ring which effectively behaves as a parallel plate capacitor. The inductance comes from the width and total length of the copper used to construct the metamaterial. Once the studied material is composed of two SRR, the total equivalent circuit will consist of two *LC* circuits. Between each layer, there is near-field coupling. Thus, the resonant polarization conversion can be tailored by the EM coupling. Around these resonant frequencies, all the field patterns will be twisted inside the slab as a consequence of interlayer coupling. [21]

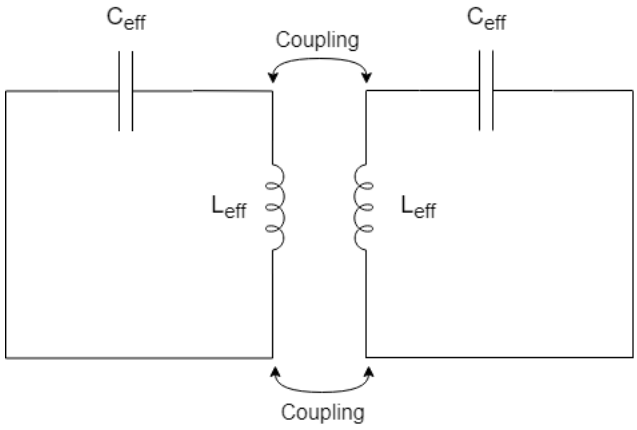

Figure 4.1: Equivelent circuit for the proposed metamaterial

Based on [6], an analysis of the electric field was performed before and after the wave traversing the medium. Assuming $\overrightarrow{E^i} = E_i^x\hat{x} + E_i^y\hat{y}$ and $\overrightarrow{E^t} = E_t^x\hat{x} + E_t^y\hat{y}$, the linear transmission matrix T_{ll} and the circularly polarized can be expressed as:

$$\begin{pmatrix} E_x^t \\ E_y^t \end{pmatrix} = \begin{pmatrix} T_{xx} & T_{xy} \\ T_{yx} & T_{yy} \end{pmatrix} \begin{pmatrix} E_x^i \\ E_y^i \end{pmatrix} = T_l \begin{pmatrix} E_x^i \\ E_y^i \end{pmatrix} \tag{4.1}$$

$$\begin{pmatrix} E_+^t \\ E_-^t \end{pmatrix} = \begin{pmatrix} E_x^t + jE_y^t \\ E_x^t - jE_y^t \end{pmatrix} \begin{pmatrix} E_x^i \\ E_y^i \end{pmatrix} = T_c \begin{pmatrix} E_x^i \\ E_y^i \end{pmatrix} \tag{4.2}$$

The two orthogonal polarization eigenstates right handed circularly polarized RCP, E_+^t, and left handed circularly polarized LCP, E_-^t, EM waves associate with the two incident orthogonal

linearly polarized components.

$$T_c = \frac{1}{\sqrt{2}}\begin{pmatrix} T_{+x} & T_{+y} \\ T_{-x} & T_{-y} \end{pmatrix} = \frac{1}{\sqrt{2}}\begin{pmatrix} T_{xx}+iT_{yx} & T_{xy}+iT_{yy} \\ T_{xx}-iT_{yx} & T_{xy}-iT_{yy} \end{pmatrix} \tag{4.3}$$

where the subscripts T_{+x}, T_{-x}, T_{+y} and T_{-y} are four transformation coefficients in the circular polarization base. The constant $\frac{1}{\sqrt{2}}$ is a result of power normalization. Note that the above equation is suitable for both cases of forward and backward propagation. Observation of equation 4.4 indicates the capability of the chiral metamaterial to transform an EM wave with linear polarization to that with circular polarization.

The transmission matrix for circularly polarized waves can also be expressed as

$$T_c = \begin{pmatrix} T_{++} & T_{+-} \\ T_{-+} & T_{--} \end{pmatrix} = \frac{1}{2}\begin{pmatrix} (T_{xx}+T_{yy})+i(T_{xy}-T_{yx}) & (T_{xx}-T_{yy})-i(T_{xy}+T_{yx}) \\ (T_{xx}-T_{yy})+i(T_{xy}+T_{yx}) & (T_{xx}+T_{yy})-i(T_{xy}-T_{yx}) \end{pmatrix} \tag{4.4}$$

As a circular polarizer for x or y-polarized incidence, the ratio $\left|t_{yx(xy)}\right| / \left|t_{xx(yy)}\right|$ should be near unity while the phase difference $\varphi(t_{yx(xy)}) - \varphi(t_{xx(yy)})$ should be around $\pm 90^\circ$ at the polarizer operation frequency.

The polarization azimuth rotation angle, θ, and ellipticity, η, of the emitted wave can be calculated by the following equations:

$$\theta = \frac{arg(E_+) - arg(E_-)}{2} \tag{4.5}$$

$$\eta = arctan\frac{|E_+| - |E_-|}{|E_+| + |E_-|} = \frac{1}{2}arcsin\frac{|E_+|^2 - |E_-|^2}{|E_+|^2 + |E_-|^2} \tag{4.6}$$

where θ is defined as the angle of the major axis of the ellipse and the x-axis, and η describes the polarization of the wave. For a pure circularly polarized wave η equals 45°, and for a pure linearly polarized wave $\eta = 0^\circ$. When η is larger than zero, the wave is left-handed, otherwise it is right-handed.

4.2 Simulation

Based on [21], the first simulations were carried out. The procedure followed to tune the operating frequency of the metamaterial was the same as to tune the Vivaldi antennas.

FEKO is a comprehensive computational electromagnetics that offers several frequencies and time domain EM solvers [22] and allowed to generate a plane wave focusing on the metamaterial and to see what was the final result, knowing, therefore, there was rotation of the electric field, and if that is confirmed, in what frequency. Periodic Boundary Conditions (PBCs) were used for the array modeling. PBCs are a set of boundary conditions which are often chosen for approximating a large system by using a small part called a unit cell simplifying the complete system design

process, as well as optimizing the time of the simulations since it allows the use of mathematics models adapted for computer simulations.

The parameters that are under evaluation are the radiation pattern and the axial ratio of the material. The objective is then to ensure that there is a rotation of the electric field at the frequency of 2.3GHz and also that the radiation pattern has characteristics that support a good transmission. In addition, the transmission coefficient was also studied in order to ensure that the maximum possible transmission efficiency exists simultaneously with the frequency of rotation of the polarization. The choice of this frequency to tune the metamaterial was due to the fact that it was one of the frequencies in which it would be possible to perform SAR tests, once the system was complete and functional, allowing not only quantification of the polarization made, but also the quality with which would fit for a real test.

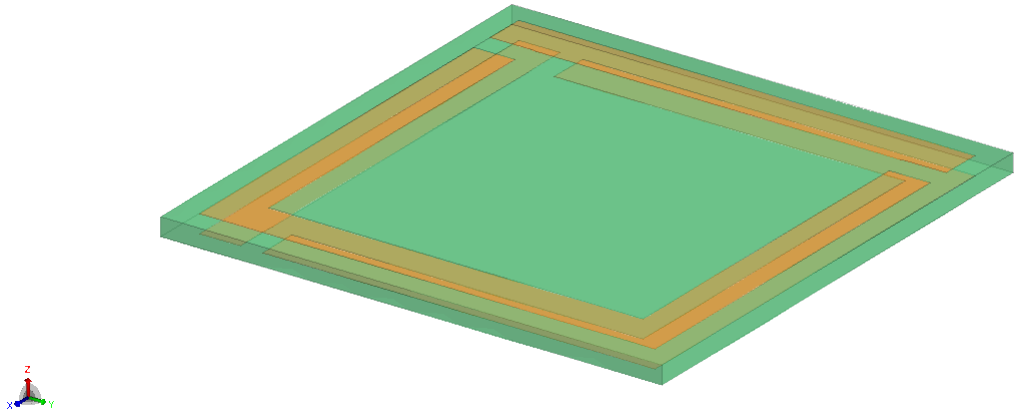

Figure 4.2: Perspective view of the unit cell structure

Initially, SRR sizes were modeled and, for this, several simulations were made where the width of the upper and lower copper layers of the rings was altered and also the size of the existing gap. As soon as a near-expected behavior was obtained, a detailed study was made of the thickness of the substrate to be used. This parameter is the key parameter in the coupling between the pair of SRRs. If the thickness is zero, no chirality will occur, since the structure is symmetric in the transmitted direction. However, if the thickness is too large, the coupling between the two SRRs is too small, each of the layers shows achirality. Thus, once the metamaterial was initially tuned, through adjustments of the copper width and gap size, several possibilities of thicknesses that could be used were evaluated, and then simulations were performed taking into account that possible values. [6]

The possible values for the substrate thicknesses available for manufacture were 1.6 mm, 1 mm and 0.8 mm.

4.2.1 Simulation to a thickness of 1.6 mm

As stated in 2.3.3, the axial ratio is the parameter that defines the degree of ellipticity of a circularly polarized wave, as such, this was the first parameter to be evaluated. The frequency range chosen for this analysis was from 2GHz to 3GHz. In this way, it would be faster computationally to obtain simulations and still maintain a good range to realize the variation in the final result by varying only the thickness of the substrate.

In figure 4.3, the axial ratio obtained with the simulation of the metamaterial with a thickness of 1.6 mm is shown in dB. This parameter will be evaluated as the ratio of the axis to the major axis, and in an ideal case, one should get as close as possible to 0dB at the frequency of 2.3GHz, and it was considered that all values above -5dB would be considered valid since they represent that a good circularity has been reached.

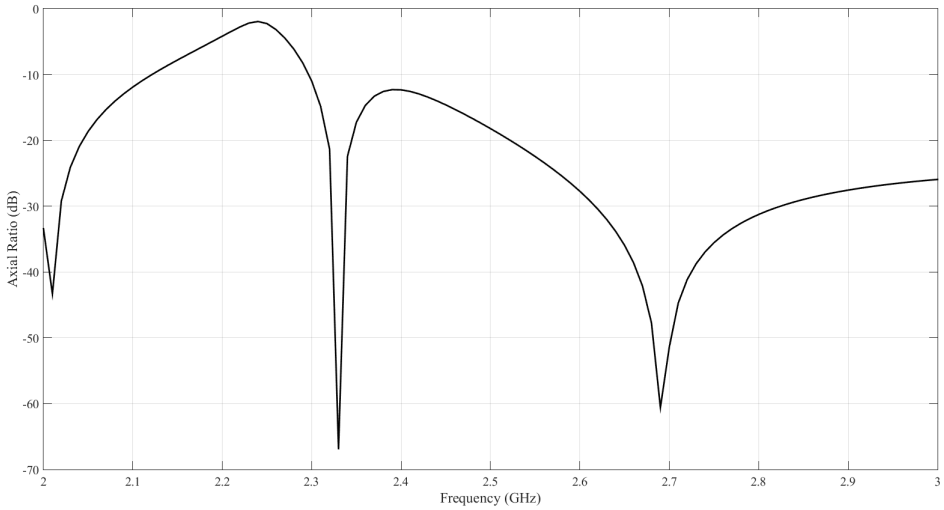

Figure 4.3: Axial ratio for a dielectric thickness of 1.6 mm

As for the transmission coefficient, shown in figure 4.4, represents the attenuation that the signal will have when crossing the metamaterial for each frequency. It is expected that at metamaterial operating frequency, the attenuation is the smallest possible since this represents that the polarization conversion is being carried out successfully and that the electric field is only being transformed and not absorbed by the substrate, or radiated to other directions.

As it is possible to prove by the simulation, the result is the expected one, that is to say, at 2.3GHz is when the attenuation is minimum, coinciding with the range in which the rotation of the polarization is being carried out, as it is verified in the figure 4.3.

The expected radiation pattern for the metamaterial is the same as for a planar antenna since the electric field from Vivaldi crosses it uniformly. The total system will, therefore, have the same behavior as a parasitic patch antenna configuration.

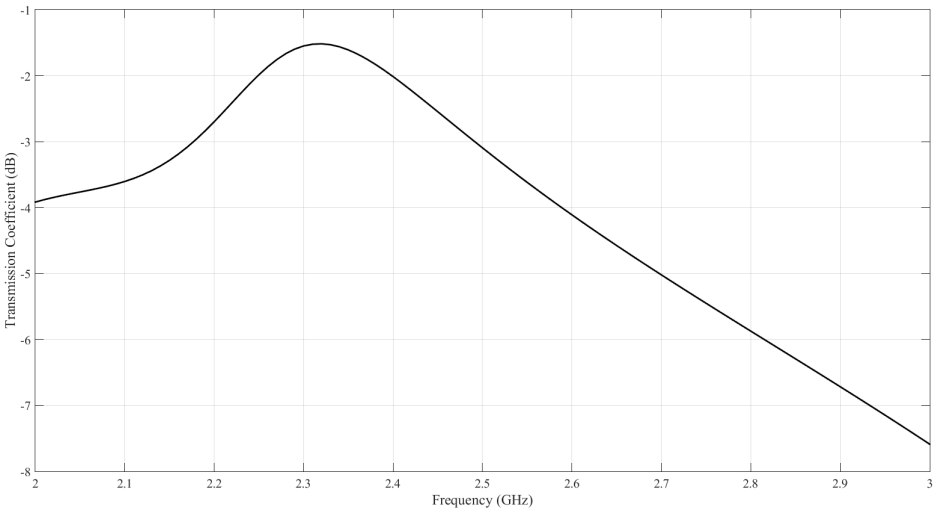

Figure 4.4: Transmission coefficient for a dielectric thickness of 1.6 mm

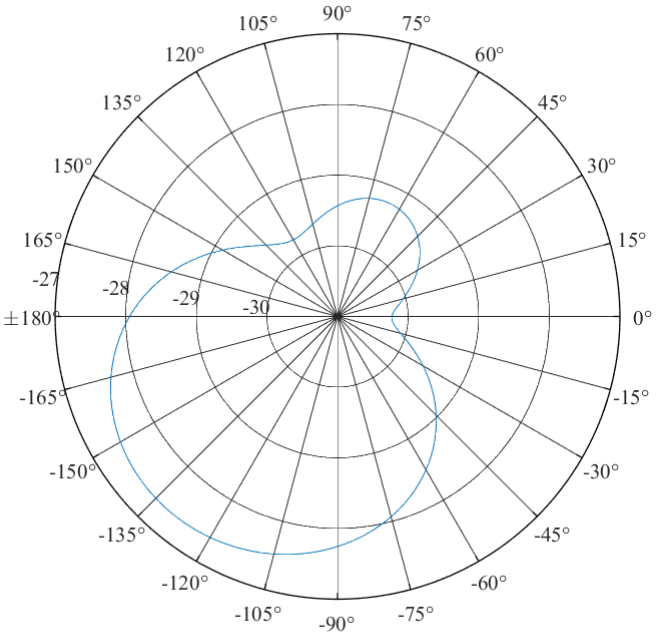

Figure 4.5: Far field plot for the metamaterial with 1.6 mm substrate thickness

By analyzing figure 4.5, it is possible to verify that the radiation pattern deviates from the desired direction of propagation, $-90°$. Such phenomenon occurs because the electric field is being confined to the substrate and, therefore, it is not possible to obtain a radiation pattern in the expected format.

4.2.2 Simulation to a thickness of 1 mm

In this subsection, it will be presented the results of the simulation in which the thickness of the substrate was changed to 1 mm, being the figure 4.6 the cartesian representation for the axial ratio and the figure 4.7 the graph for the transmission coefficient.

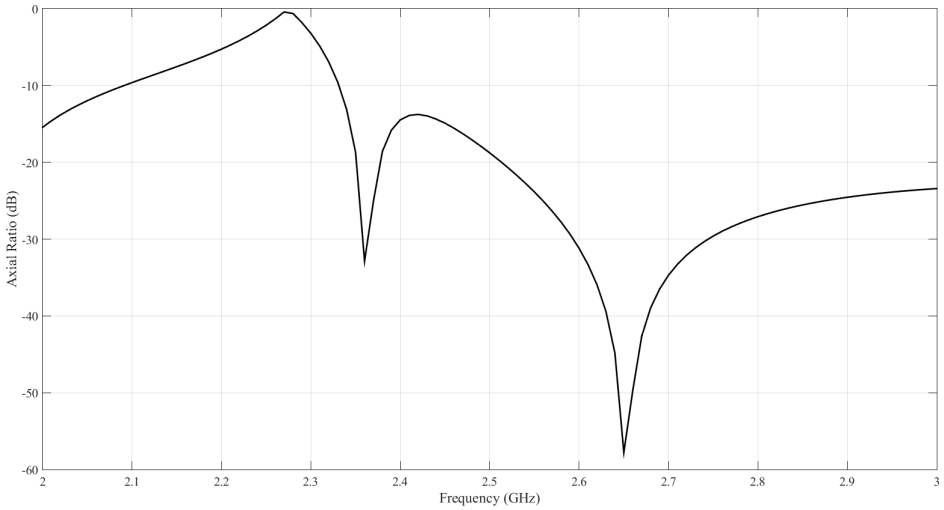

Figure 4.6: Axial ratio for a dielectric thickness of 1 mm

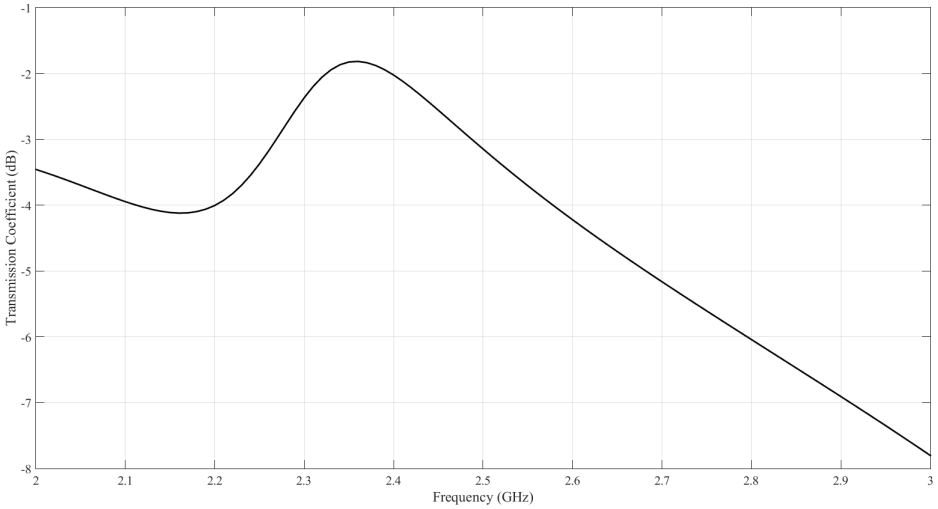

Figure 4.7: Transmission coefficient for a dielectric thickness of 1 mm

Observing the obtained results, it is again verified that there is a high correlation between the values at which the polarization transformation occurs and the results of the attenuation. Comparing the obtained results with those of section 4.2.1, it is possible to verify that the reached value for the axial ratio has been improved since a small deviation occurred at the frequency at which

the maximum value occurred. For the transmission coefficient, the same deviation occurs, in the same order of magnitude when compared to the axial ratio, even so, the value of the minimum attenuation reached is similar, however, it occurs at a slightly higher frequency. The presented values for both the axial ratio and the coefficient of transmission are very satisfactory.

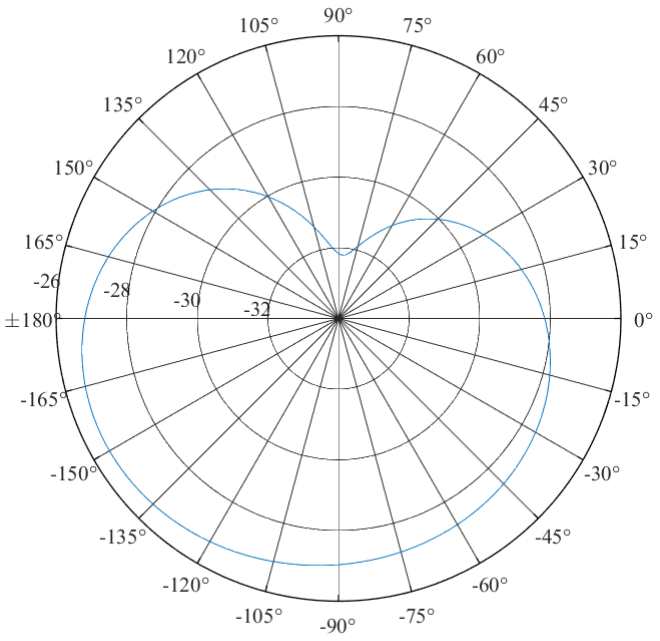

Figure 4.8: Far field plot for the metamaterial with 1 mm substrate thickness

In figure 4.8 is represented the polar graph representative of the radiation standard of the antenna. It is then possible to verify that the radiation pattern is already more in agreement with what is intended, that is to say, to present a good distribution of the electric field. In this way, it is possible to ensure that the energy coming from the array continues its path without any deviation.

4.2.3 Simulation to a thickness of 0.8 mm

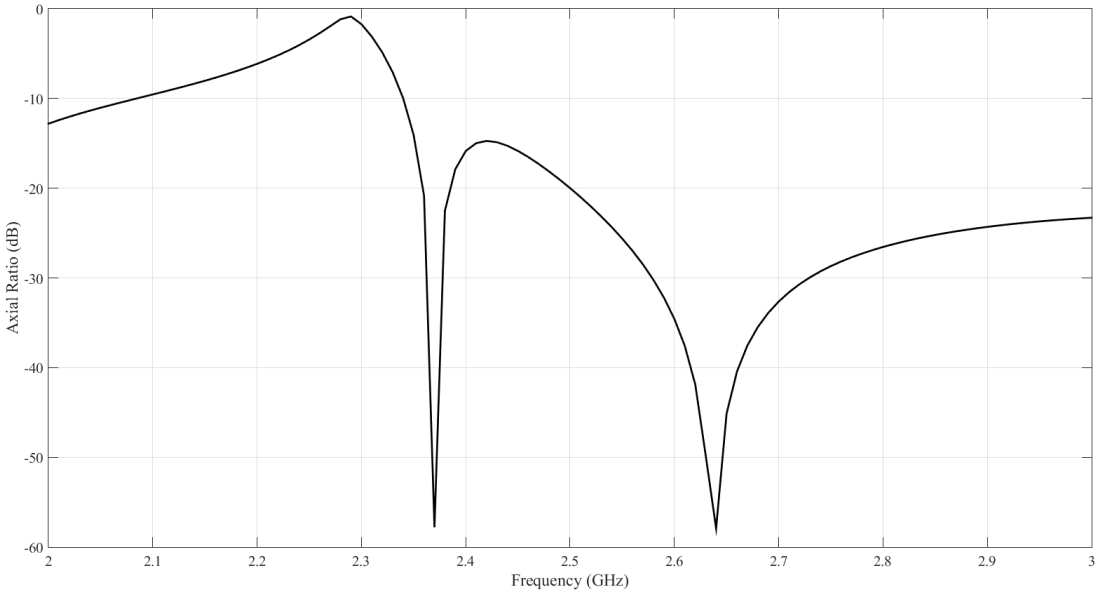

Figure 4.9: Axial ratio for a dielectric thickness of 0.8 mm

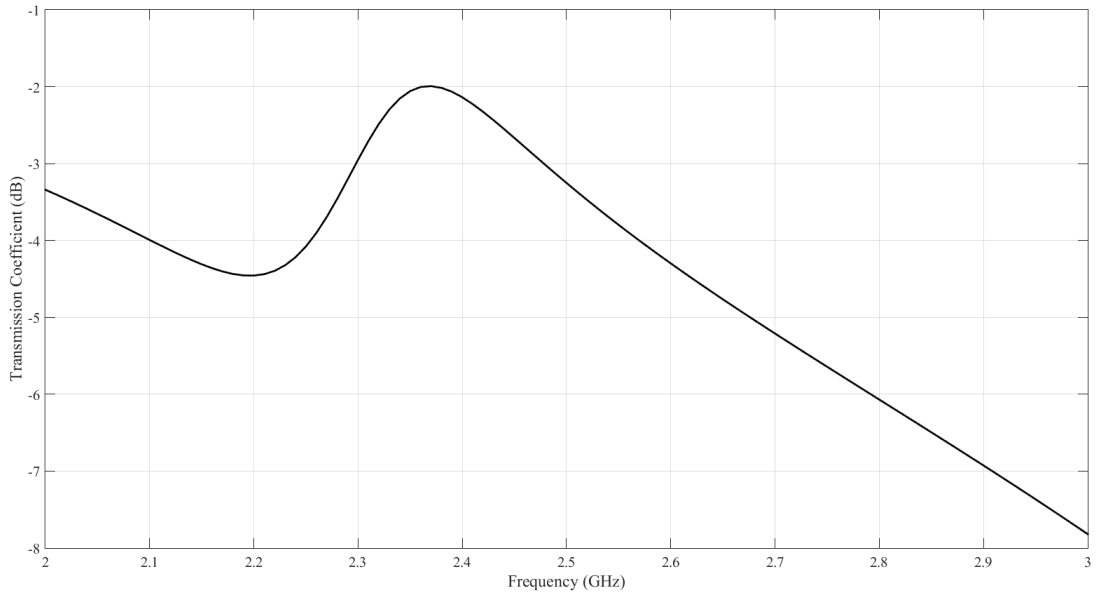

Figure 4.10: Transmission coefficient for a dielectric thickness of 0.8mm

After having chosen to use a thickness of 0.8 mm for the substrate, a deeper analysis was made regarding the behavior of the metamaterial. First, it was checked the circulation of currents in the two different copper layers to observe the coupling between the electric and magnetic fields.

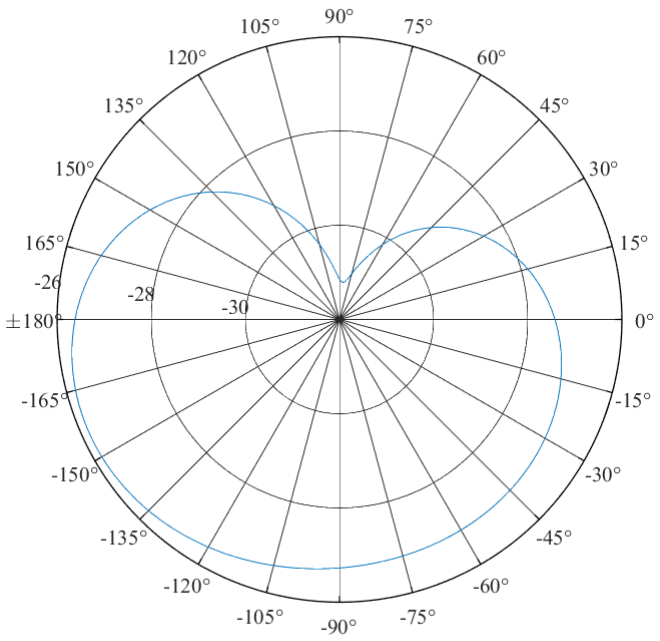

Figure 4.11: Far field plot for the metamaterial with 0.8mm substrate thickness

The final analysis was again to the radiation pattern of the metamaterial, shown in figure 4.11. It is possible to verify that this is very similar to the case in which the thickness is 1mm, so it will not be a differentiating factor for the choice of the final thickness for the metamaterial. The fact that the radiation pattern is similar is due to the thickness difference being the only 0.2 mm, which does not cause a big difference in the electric field being confined in the substrate.

Since the thicknesses 1 mm and 0.8 mm were the closest ones to what was intended, they were the solutions that were developed and characterized in order to implement next to the array.

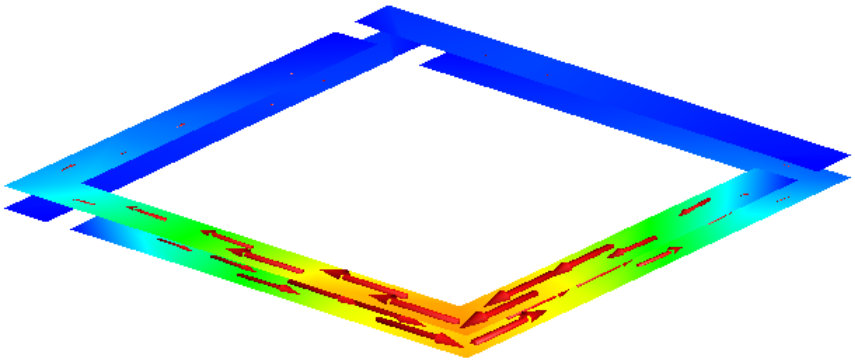

Figure 4.12: Current distribution view of the unit cell structure at 2.3GHz

The currents on the front and back SRRs are in antiparallel direction on the top and bottom

layers of the structure which corresponds to an asymmetric resonance mode as coupled magnetic dipoles. Thus, the near-field coupling mode of the first and second SRRs can be excited efficiently, resulting in an emitted RCP or LCP wave at resonances. If the currents on the front and back SRRs were in the same direction, symmetric resonance mode as coupled electric dipoles resonance and the fundamental electric resonance mode of the first SRR could be excited efficiently.

In addition to studying the behavior of the metamaterial at 2.3GHz, it was also studied the behavior of metamaterial from 2GHz up to 8GHz, which is the range of frequencies covered by the antenna, using for simulation the case of having a thickness of 0.8mm

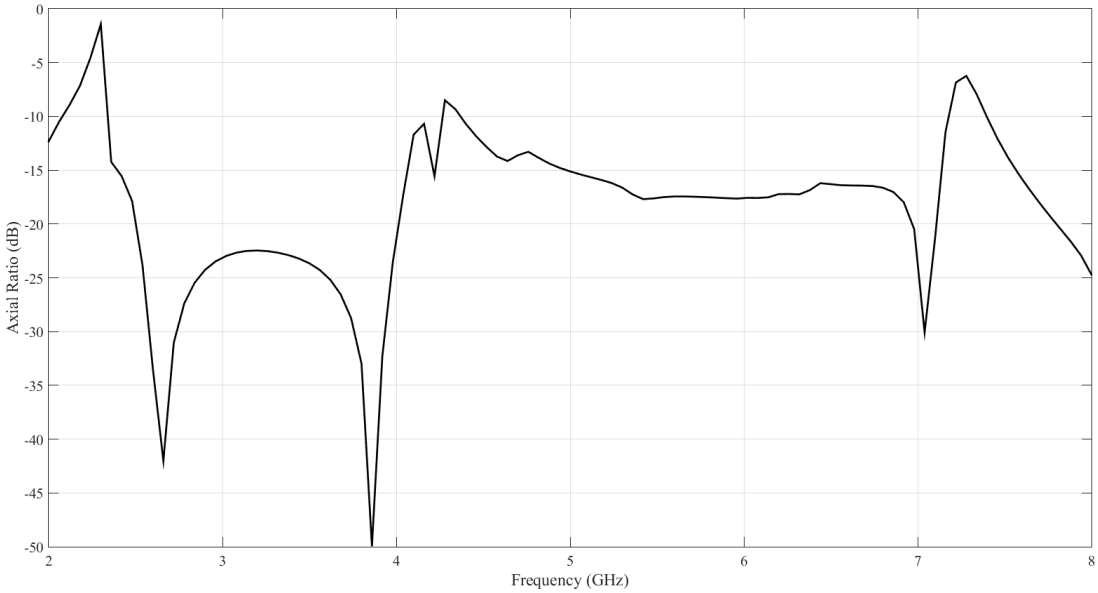

Figure 4.13: Axial ratio for a complete frequency range analysis

Analyzing figure 4.13 and 4.14, it is possible to verify that there are three possible points of interest for the metamaterial drawn, even though two of these points are outside the range of frequencies that can be used in a real case. The first point of interest is in the case of 2.3GHz which has been studied and explained in this subsection. The second point of interest occurs at the 4.2 GHz frequency. At this point, it is verified that the value of the axial ratio increases largely, reaching -5dB and, at the same time, the value of the coefficient of transmission for that same frequency also reaches a local maximum.

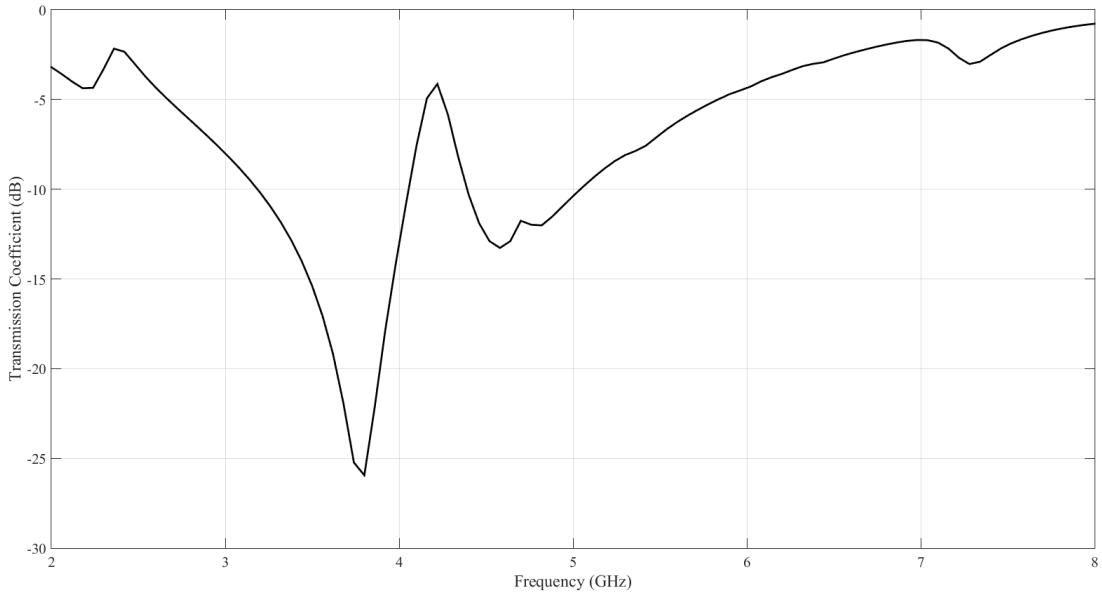

Figure 4.14: Transmission coefficient for a complete frequency range analysis

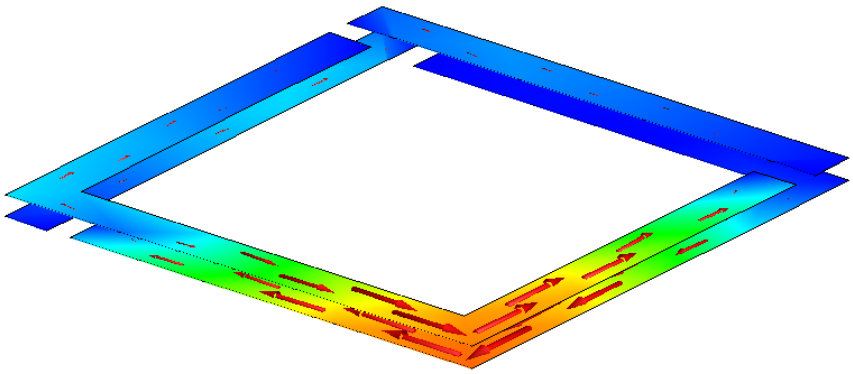

Figure 4.15: Current distribution view of the unit cell structure at 4.2GHz

Analyzing the distribution of currents on the surface of the rings, a similar behavior occurs in the case shown in figure 4.12. The difference is in the direction of the currents, which indicates that in case of having LCP at 2.3GHz, 4.2 GHz we will get RCP or the reciprocal case. However, it is noteworthy that at this frequency the maximum value reached by the axial ratio is -10dB, which would not be used since it was considered that the value of this parameter would have to be at least -5dB for consider having a good circularity for the intended application.

The third point of interest is around 7.2GHz. At this frequency, the axial ratio has a sharp drop, followed by an abrupt rise, thus having a minimum and maximum locations in a narrow range of frequencies.

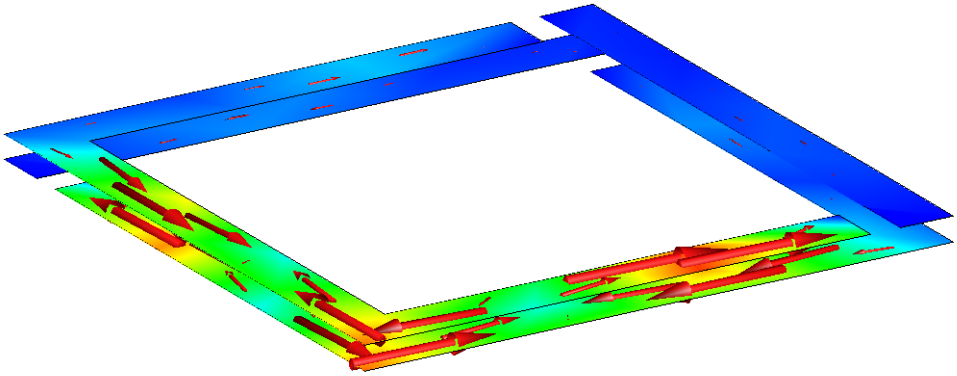

Figure 4.16: Current distribution view of the unit cell structure at 7.1GHz

Again, an analysis of the distribution of currents shows that at 7.1GHz there are anti-parallel currents in the right and bottom branches of both rings of the structure, which causes an induced magnetic field. Then the electric field that penetrates the metamaterial would be excited by the magnetic field, resulting in the cross-polarization transmission for the linear polarized incident wave propagating along the direction of propagation. This behavior indicates that one is facing a linear polarization transformer, known as the giant optical rotation. According to the 4.13 and 4.14 images, it is then possible to conclude that at the 7.1 GHz frequency a linear polarization can be transformed into its cross polarization with only a 2 dB attenuation.

In the 7.2GHz analysis, a similar behavior was observed in the case of 4.2GHz, that is, a transformation from linear to circular, but with an axial ratio in the order of -6dB, which, although a better value of than 4.2GHz, is still insufficient to be able to be used in SAR applications.

Chapter 5

System integration and testing

The base of the system consists of the array of thirty-two antennas as well as their feeding network. In the next subsections will be presented the characterization of the system in terms of S-Parameters as well as in terms of system radiation pattern performed in the faculty's anechoic chamber. In addition, this characterization was made to some variations of the system, which includes the insertion of the metamaterial and a metallic box that will serve as support in real tests of the system. Results concerning this tests are shown and conclusions are drawn out of them. It should also be noted that in the future this system may be applied in real SAR situations for a frequency of 2.3 GHz, as such, throughout this chapter, the emphasis will be given for this frequency.

5.1 Antennas array

The anechoic chamber at Faculty of Engineering of University of Porto was the required place for measuring the radiation pattern of the array, and subsequently its gain and circularity. It is the ideal place to measure those parameters, because of its special conditions in absorbing EM waves, in order to avoid their reflections. An antenna acting as a transmitter and an Antenna Under Test (AUT) form the essential predicate to obtain radiation pattern measurements. The array worked as an AUT.

The first characterization made was the array since it is the main cell of the whole system, starting by measuring the values of the S-Parameters of the array.

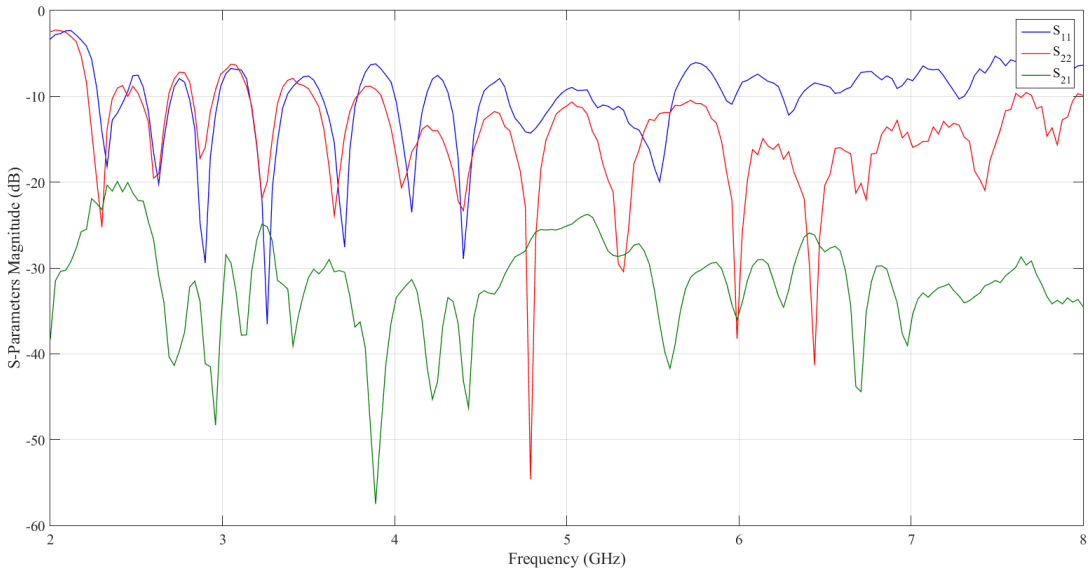

Figure 5.1: S-Parameters of the array

As can be seen for port 1, starting at 5.7 GHz, it starts to perform differently than expected when compared to simulation results. This effect may be due to the transmission lines that feed this port to have small inaccuracies during the construction, which may have altered its characteristic impedance, affecting mainly the high frequencies. The fact that for port 2 and the coupling factor between antennas remains similar to the simulated one, the hypothesis of fluctuations in the relative dielectric permittivity of the substrate was excluded.

This system was also characterized by the measurement of its realized gain. For this, the substitution method was used. As exemplified in figure 5.2, the first measurement made was the S_{21} and the distance between two antennas of Vivaldi in the anechoic chamber. The distance allowed to calculate the losses of free space between the antennas through the equation 5.1.

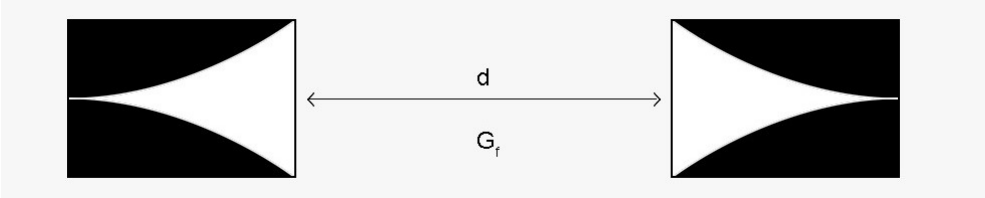

Figure 5.2: Exemplary schematic of the measurement performed between the two Vivaldi antennas

$$G_f = \left(\frac{\lambda}{4\pi R}\right)^2 = \left(\frac{c}{4\pi R f}\right)^2 \tag{5.1}$$

Since the antennas were spaced 4.15 m apart, the associated free space losses are 52.04 dB at a frequency of 2.3 GHz.

After the measurement with the two Vivaldi antennas to be performed, the two antennas were measured, this time using a Log-Periodic antenna as a reference, as shown in figure 5.3.

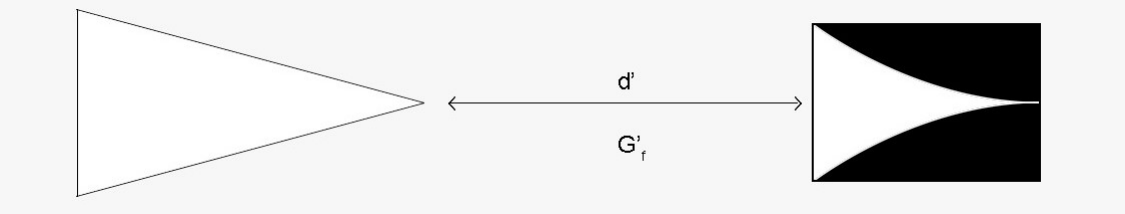

Figure 5.3: Exemplary schematic of the measurement performed between the two Vivaldi antennas and the Log-Periodic antenna

With the equations' system 5.2, it is possible to withdraw the gain values of each of the antennas.

$$\begin{cases} G_{Viv_B} = G_{Viv_A} + \Delta G \\ G_F + 2G_A + \Delta G = M_{viv_A viv_B} \end{cases} \tag{5.2}$$

where $M_{viv_A viv_B}$ is the S_{21} measure between Vivaldi A and B and ΔG is the difference between the measured S_{21} between the two Vivaldi and Log-Periodic, that is, $M_{viv_A LP}$ and $M_{viv_B LP}$.

Once the above system is solved, it is then possible to determine the relationship between the gain of the Log-Periodic antenna and the losses of free space between this antenna and the Vivaldi. Note that the distance will be different since the Log-Periodic antenna has a different length than the Vivaldi antenna.

$$\begin{cases} G_{LP} + G_{F'} = M_{viv_A LP} - G_A \\ G_{LP} + G_{F'} = M_{viv_B LP} - G_B \end{cases} \tag{5.3}$$

After these measurements were made and the value of the gains and their relationship to the losses were known, the Vivaldi antennas were replaced by the array to know what his gain is as exemplified in figure 5.4.

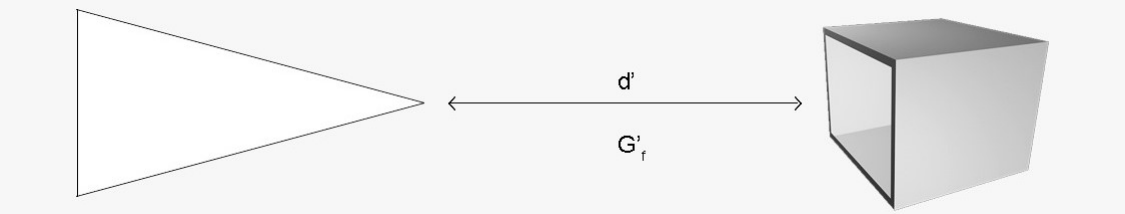

Figure 5.4: Exemplary schematic of the measurement performed between the array and the Log-Periodic antenna

Using equation 5.4, it is then possible to calculate the gain of the array.

$$G_{array} = M_{arrayLP} - (G_{LP} + G_{F'}) \tag{5.4}$$

In order to create the 3D radiation pattern of the system to be clearer where the array radiates its energy, the antenna was rotated following two different axes independently, firstly about the axis that goes from one antenna to the other from 0° to 180° in steps of 12° , and next about the

vertical axis perpendicular to the floor from $-90°$ to $90°$ in steps of $5°$, as demonstrated in figure 5.5.

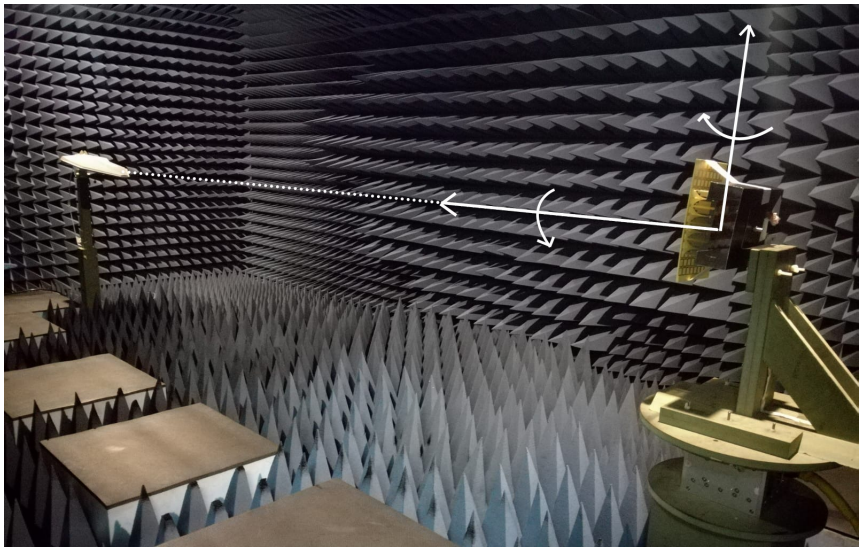

Figure 5.5: Graphical representation of rotation axes

In figures 5.6 it is possible to observe the radiation pattern for a linearly polarized wave for port 1, and in figure 5.7 the radiation patterns for the same polarization is again demonstrated, this time for port 2.

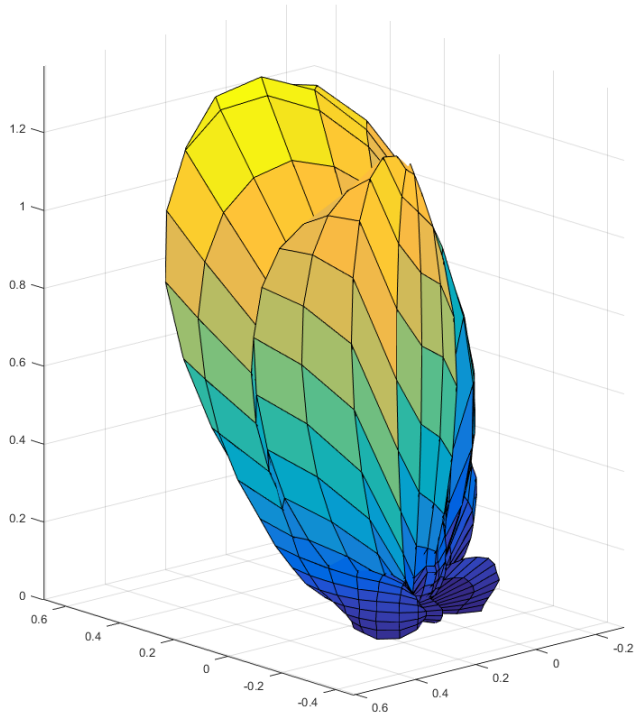

Figure 5.6: 3D measured radiation pattern for a linearly polarized wave for port 1

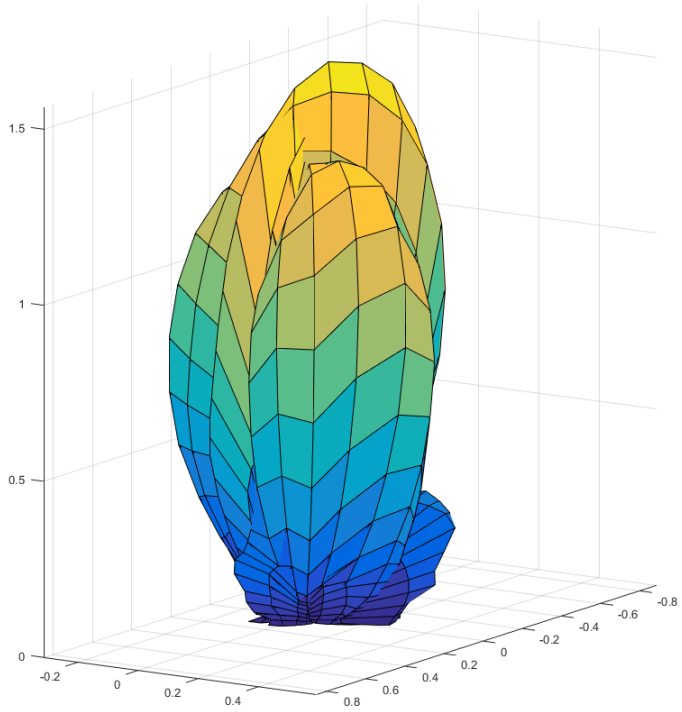

Figure 5.7: 3D measured radiation pattern for a linearly polarized wave for port 2

By analyzing both the radiation patterns, they are found to be similar, as expected. However, having a radiation beam not as narrow as desired and being simulated will cause the gain value to be adversely affected. In addition, it is possible to verify that the radiation pattern presents sidelobes, that is, the array is radiating part of its energy to the sides, which will also contribute to a decrease in the gain value. Finally, from the analysis made to the obtained radiation patterns, it is verified that essentially in port 1, figure 5.6, the energy is being radiated with a deviation from the desired direction. This phenomenon causes that the antenna should not be pointed directly to the desired location but rather with a small deviation, which can be a disadvantage to be used for RADAR and SAR at long distances, as it may be difficult to focus on the target. The maximum gain obtained for the array was 4.5 dBi.

5.1.1 Antennas array with metamaterial and metal box

The second characterization made was the array integrated with its mechanical support together with the metamaterial. Tests were performed where the distance between the metamaterial and the array was varied, and it was verified that the best performance happened when this distance was minimum, that is, the metamaterial was immediately after the array. The system antennas array with metamaterial and metal box is the one that is intended to be integrated into real SAR systems, as such it was important to characterize it. It is also important to characterize the behavior of this system because it is expected that this will not vary significantly depending on where it is inserted

since the box will also serve as shielding for the remaining medium. So, just attach the array to the device that will support the SAR system and is ready for use.

The box was made of metal material so that it could be easily integrated with other systems, such as the structure of an airplane. To facilitate this integration, rails have been placed in the back of the metalic box that serve as support. Figure 5.8 shows a 3D view of how the box and array are integrated, and figure 5.9 shows the detail of the rails.

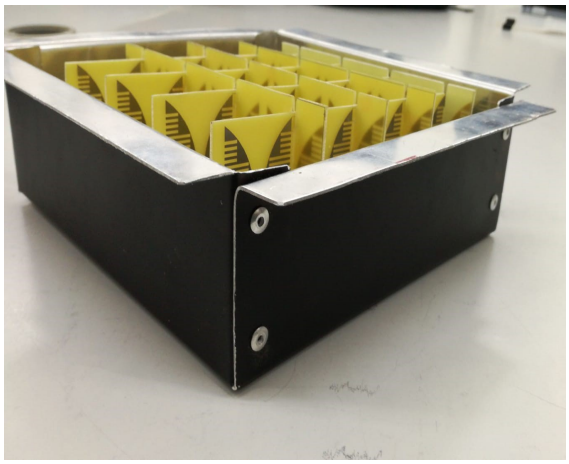

Figure 5.8: 3D view of the fully integrated system

Figure 5.9: Back of the metalic box together with rails

It was then initially started again by measuring the values of the S-Parameters of the array with metamaterial and the box.

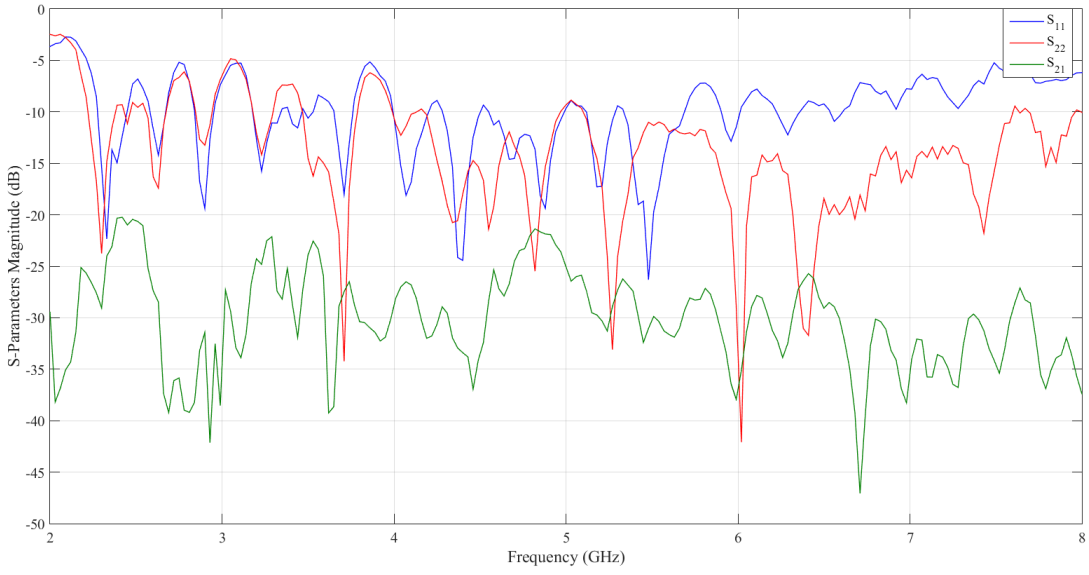

Figure 5.10: S-Parameters of the array with metamaterial and the box

Comparing the S-Parameters of the array with the array, box, and metamaterial, it is verified that there are no significant changes, either in the reflection coefficient of each port or in the coupling factor between ports. In fact, whatever the frequency to be used, each port has at least 20 dB isolation between them, which meets the initial requirements. An important fact to note is that several distances were tested for the metamaterial to be in the array and that it was concluded that the position immediately after the array did not present problems even in the near-field region. This data helps to make the system even more compact because it was expected that the metamaterial would be placed about 25 cm from the array to be already in the far-field zone of the array.

Next, the system's radiation pattern was again characterized. In figures 5.11 and 5.12 it is possible to observe the radiation pattern for both circular polarizations for port 1, while in figures 5.13 and 5.14 the radiation pattern for circular polarizations is again demonstrated, this time for port 2.

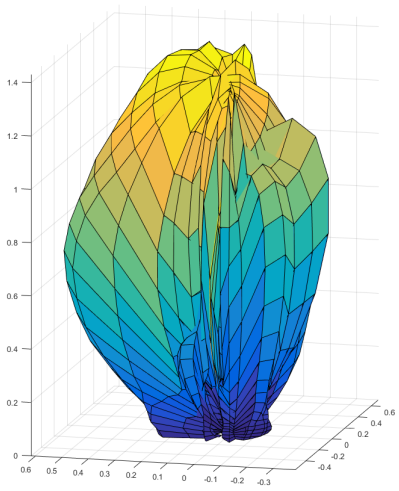

Figure 5.11: 3D measured radiation pattern for the LHCP for port 1

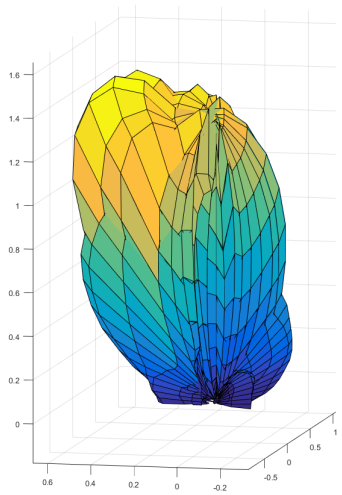

Figure 5.12: 3D measured radiation pattern for the RHCP for port 1

After analyzing the radiation patterns, it is verified that the gain of the system with the box is superior to that of only the array, even this one having the metamaterial to attenuate its signal. This is due to the fact that there are no sidelobes and possibly backlobes in the system because the array is involved in a conductive plane, which causes the energy to be radiated forward. Even so, the radiation beam is not as narrow as desired, so there are still losses in gain. The maximum gain obtained for the system in this configuration was 5.9 dBi, however, considering that we are facing circular polarization the gain is 2.9 dBi.

Another analysis was the axial ratio of the system because it was important to analyze the circularity obtained, in order to study if the metamaterial has the desired behavior. In figure 5.15 the value of the axial ratio for the analyzed frequency range is shown.

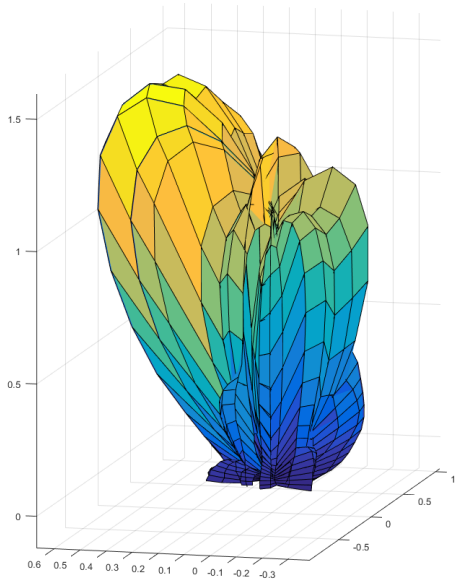

Figure 5.13: 3D measured radiation pattern for the LHCP for port 2

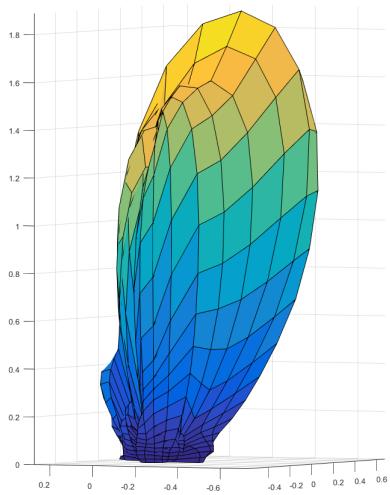

Figure 5.14: 3D measured radiation pattern for the RHCP for port 2

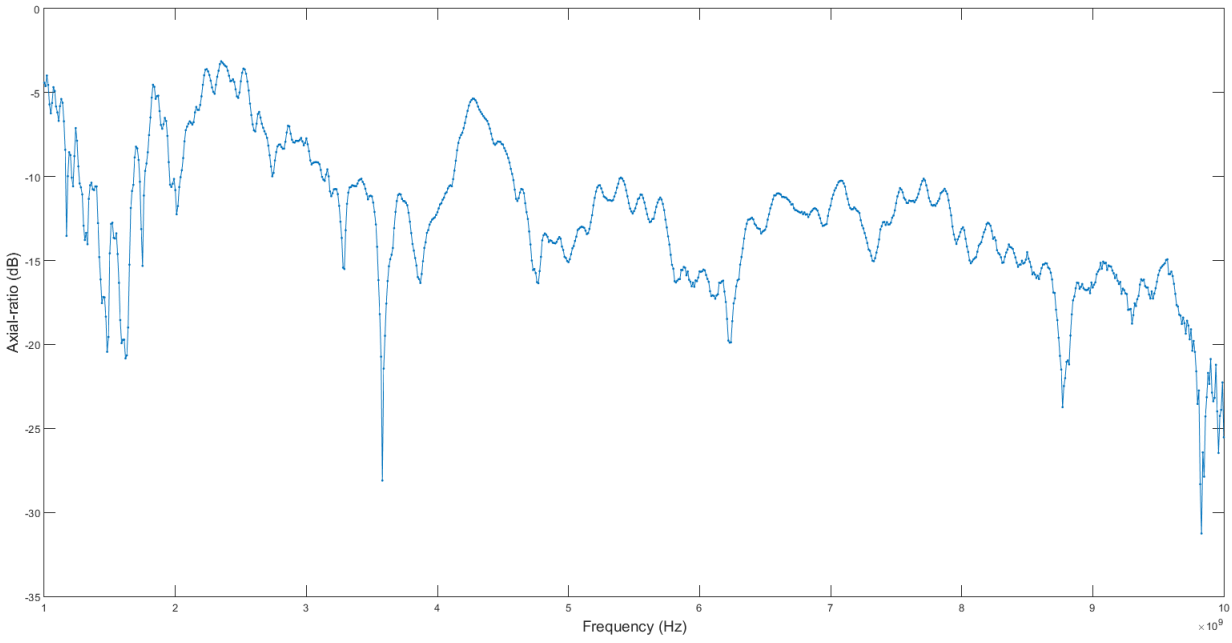

Figure 5.15: Measured axial ratio of the system

The numerical simulation is in good agreement with the measured results, which reveals that circular polarized wave emissions can be obtained from linearly polarized waves in two different bands obtained simultaneously at microwave frequencies. As such, it is found that the metama-

terial has the desired effect in the 2.3GHz band, that is, it is transforming a linear polarization into a circular one. Although the value is not as close to 0 dB as the simulation showed, the frequency range above -5 dB, which was considered acceptable for the application, is higher than the simulated one. In addition to the frequency of interest, it is verified that at the frequency of approximately 4.2GHz, there is an increase of the axial ratio, which again is against the simulated effect.

5.1.2 Antennas array with metamaterial

In order to study the influence of the box on the system, the gain of the array and its radiation pattern with only the metamaterial were analyzed again.

The analysis done initially was again that of the S-Parameters of the system under analysis.

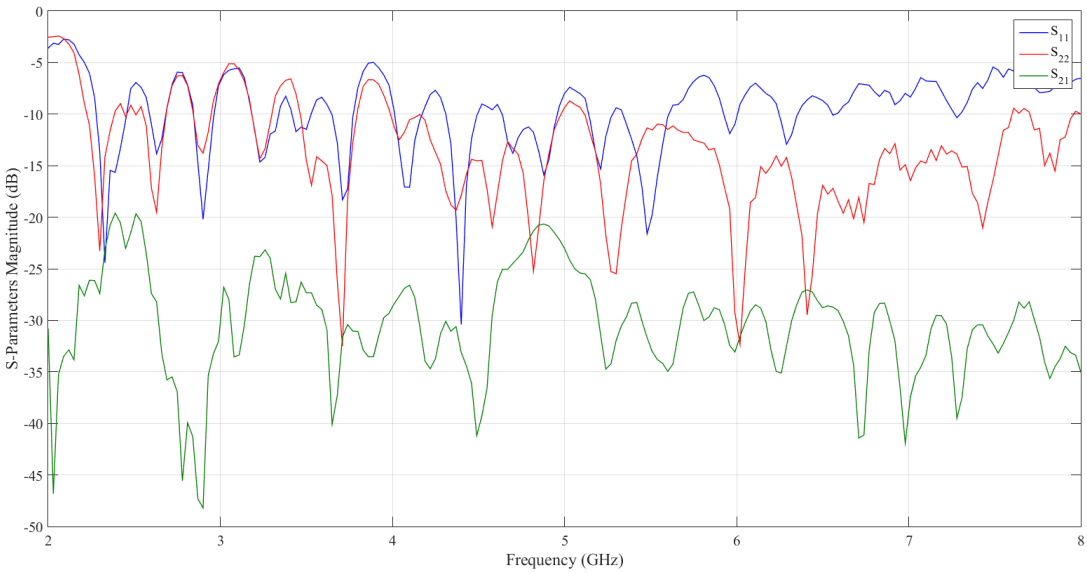

Figure 5.16: S-Parameters of the array with metamaterial and the box

Again, and as expected, the S-parameter measurements are similar to those previously reported, ie, port 1 continues to have a defect as compared to the simulation for the 5.7 GHz frequency, and the remaining measurements are similar to each other and with the results of the simulations. It can be concluded that the insertion of the metamaterial and the metal box next to the array does not harm the magnitude of the S-Parameters.

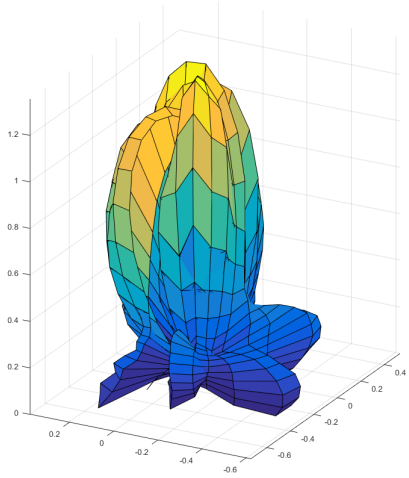

Figure 5.17: 3D measured radiation pattern for the LHCP for array with metamaterial for port 1

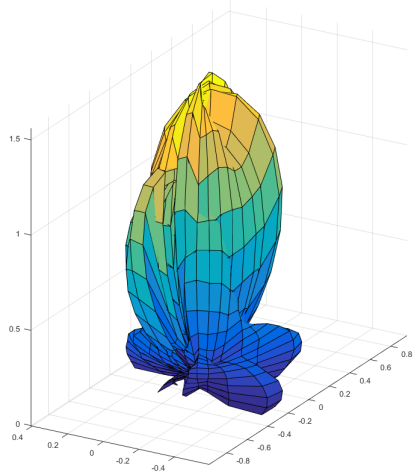

Figure 5.18: 3D measured radiation pattern for the RHCP for array with metamaterial for port 1

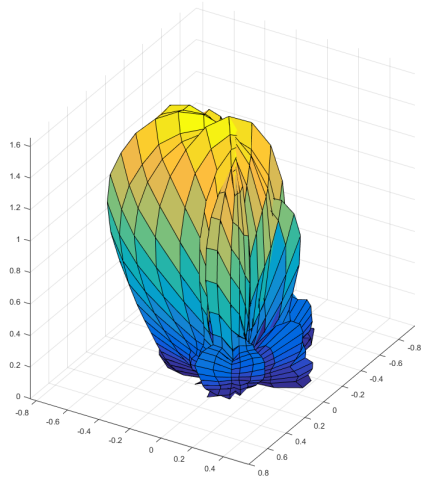

Figure 5.19: 3D measured radiation pattern for the LHCP for array with metamaterial for port 2

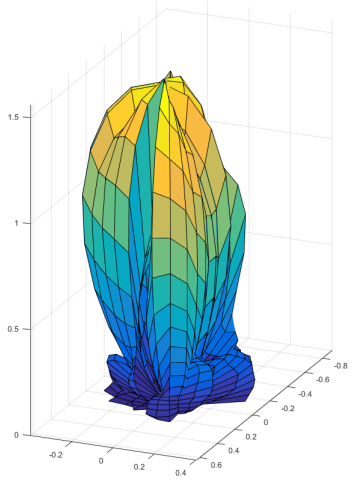

Figure 5.20: 3D measured radiation pattern for the RHCP for array with metamaterial for port 2

By analyzing the system composed of the array and the metamaterial, it is possible to verify the presence of sidelobes in the system and consequently loss of gain when compared to the same system with a metal box. The maximum gain obtained for the system in this configuration was 4.4 dBi however, considering again that we are facing circular polarization the gain is 1.4 dBi.

5.2 Metamaterial characterization

As already mentioned, the purpose of using the metamaterial was to overcome the fact that the antennas are in cross-polarization, making it difficult to get a good SAR operation. So, to make a linear polarization in a circular it was used a metamaterial. In order to test the material with 0.8 mm of thickness, two Vivaldi antennas were used and four measurements were taken: each of the antennas was placed horizontally and vertically, making combinations of their position with each other, as shown in table 5.1.

Table 5.1: Combination of antennas with each other.

0º	0º
90º	0º
0º	90º
90º	90º

considering that 0° is when the antenna is in a horizontal position and 90° for the vertical one.

The procedure for data processing involves making a combination of the phases of the various signals sent and received in order to understand whether there is a rotation of the polarization. In figure 5.21 is represented the polarization analysis made for the metamaterial. The first two elements, vertical to RHCP and vertical to LHCP, represent the right and left circular transformation for a linear transmission with the antenna vertically. The horizontal to RHCP and horizontal to LHCP plots represent the same transformation only this time for a linear transmission with the antenna horizontal.

By doing a general analysis of the system, it is possible to verify that, as in simulation, the 2.3GHz and 4.2GHz frequencies are strong evidence of polarization rotation. This is due to a difference of about 12dB between the RHCP and LHCP components. In addition, it is possible to verify that, at 2.3GHz, vertical polarization is being transformed into LHCP and horizontal in RHCP. At 4.2GHz, as was simulated, the opposite case occurs however not in one way, that is, the vertical polarization is transformed into RHCP and the horizontal into LHCP, although with a difference of less than 2.3GHz in the order of 10dB, for the LHCP and RHCP biases, respectively for the vertical and horizontal case.

In order to better understand the phenomenon present, a zoomed into the zone of interest in the 2.3GHz interest range is presented.

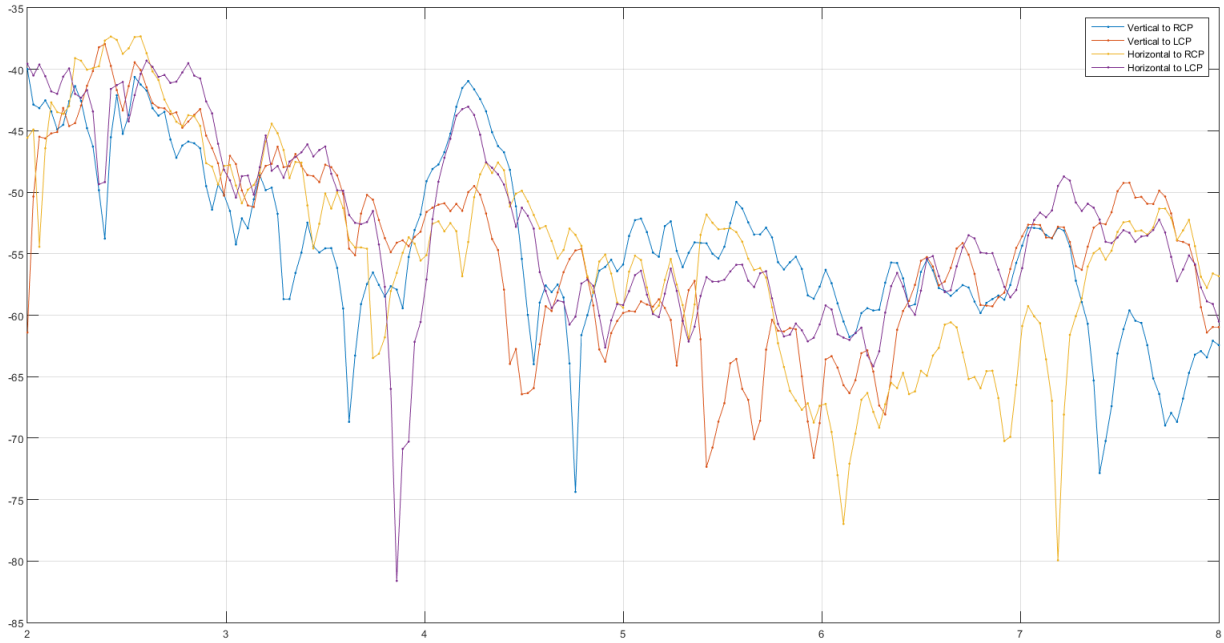

Figure 5.21: Measured linear to circular transmission coefficients

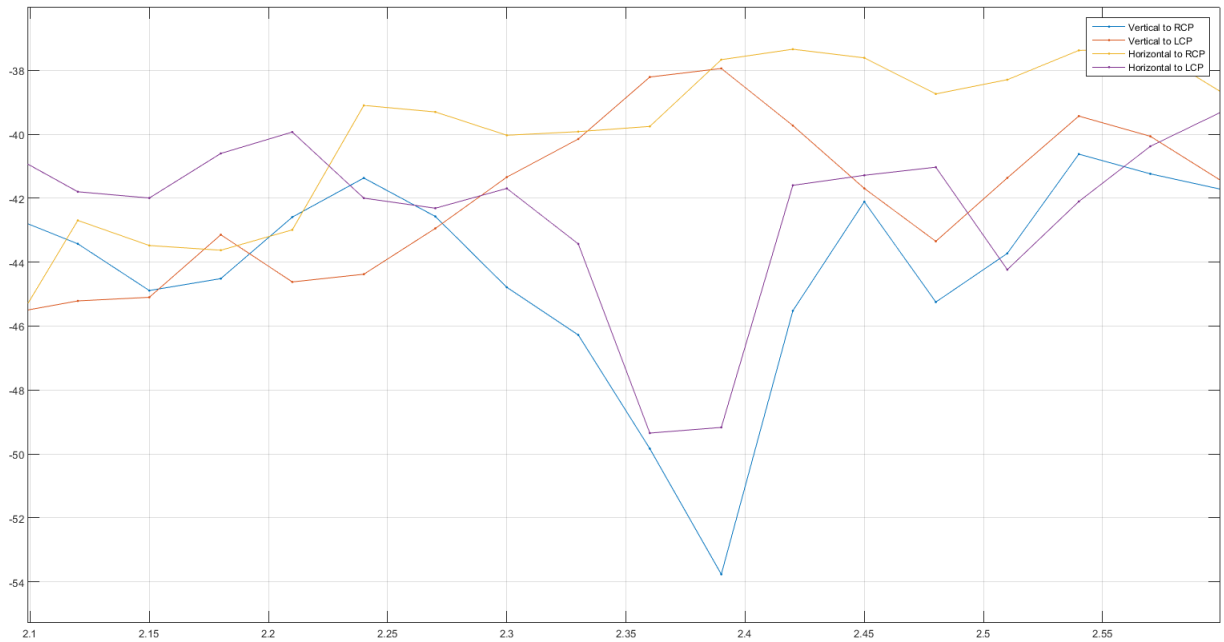

Figure 5.22: Measured linear to circular transmission coefficients to the frequency range of 2.3GHz

Analyzing figure 5.22, it turns out that the polarization rotation is occurring, however with a small deviation when compared to the simulation. This deviation may have occurred due to

inaccuracy regarding the electric permittivity of the FR4 substrate. In addition, the method of manufacture may also have influenced the resonance frequency of the metamaterial since the slot rings resonators were not perfectly aligned, as was simulated.

Even with a 100MHz deviation in the operating frequency of the metamaterial, it can be verified that it has the desired effect. With these conclusion it is possible to state that the results are very good.

5.3 Analysis of the Results

As mentioned in the previous subsection, the gain value of the array was lower than the expected one. As such, some simulations and a detailed analysis of the results were carried out, in order to understand the causes.

The first analysis was the transition of the antenna to its feeding network. Since vias, the wire that connects the antenna to the PCB and even the solder have an inductive effect, one studied the behavior that this inductance causes in the energy that reaches the antenna and in the phase shifts that this causes between feeds. For this, an inductor was placed between the antenna and the port that feeds it by varying its inductance, as shown in figure 5.23.

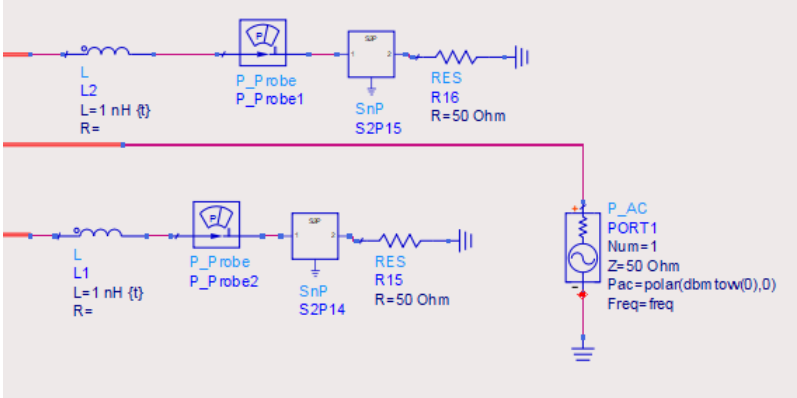

Figure 5.23: Simulation of losses in the substrate and lines focusing on 2 ports

The inductance induced by a wire can be calculated using 5.5 while that induced by a via is calculated using the equation 5.6.

$$L_{wire} = 2l\left\{ln\left[\left(\frac{2L}{D}\right)\left(1+\sqrt{1+\left(\frac{D}{2L}\right)^2}\right)\right]-\sqrt{1+\left(\frac{D}{2L}\right)^2}+\frac{\mu}{4}+\left(\frac{D}{2L}\right)\right\} \tag{5.5}$$

$$L_{via} = 5.08h\left[ln\left(\frac{4h}{d}\right)+1\right]nH \tag{5.6}$$

The total calculated inductance is approximately 8 nH. This value was attributed to the inductances placed in the simulation and it was verified that the total power arriving at each port was

2.7×10^{-5} W, corresponding to -15.33 dBm, which means that each antenna has a total gain loss of 3.33 dB, rather than 2,26 dBm as initially expected.

After the power losses analysis, a study was made of the influence that the inductors have on the phase of the signal arriving at each port of the antenna. In figure 5.24, the signal phases of the various antenna ports are represented.

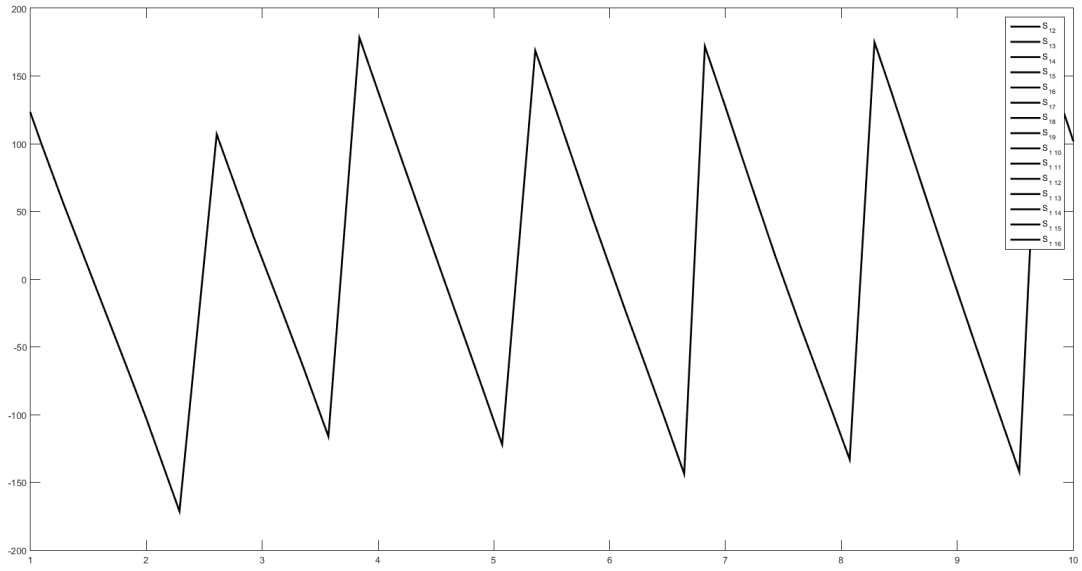

Figure 5.24: Phase differences simulation between antenna feeding ports

As can be seen, as expected, there is no phase shift when there is an inductance of equal value between the different ports of the PCB to the antennas. However, the wires connecting the antennas to the PCB may have a small variation in length, making their inductance vary, however, this variation is trace, such as the phase change caused. However, a simulation was performed in the HFSS where each antenna port had a phase shift of 1° degree between the previous and, even with this exaggerated situation, these phase shifts were not significant for the array's radiation pattern.

Another factor that justifies the loss of gain of the complete system is that the metamaterial causes a reduction in the gain of the array. According to the simulation, it was possible to verify that in the operation frequency of the metamaterial, 2.3GHz, it would have an attenuation in the order of 2 dB, however, measured values show that the actual operating frequency happens at 2.4GHz. Considering that the metamaterial has an offset of 100MHz comparing the measured value from the simulated one, it is verified that the value for the 2.2GHz attenuation in the simulation is 4.3 dB, and it is estimated that this is the loss that the element causes on the system.

A parameter also analyzed was the axial ratio of the array without metamaterial. The expected result would be to have a linear polarization for the frequency of 2.3GHz for the different variations of rotation of the array. However, the array could be implementing circular polarization without

this being intended, leading to loss of gain. Figure 5.25 shows the measured and simulated result of the axial ratio for the 2.3 GHz frequency.

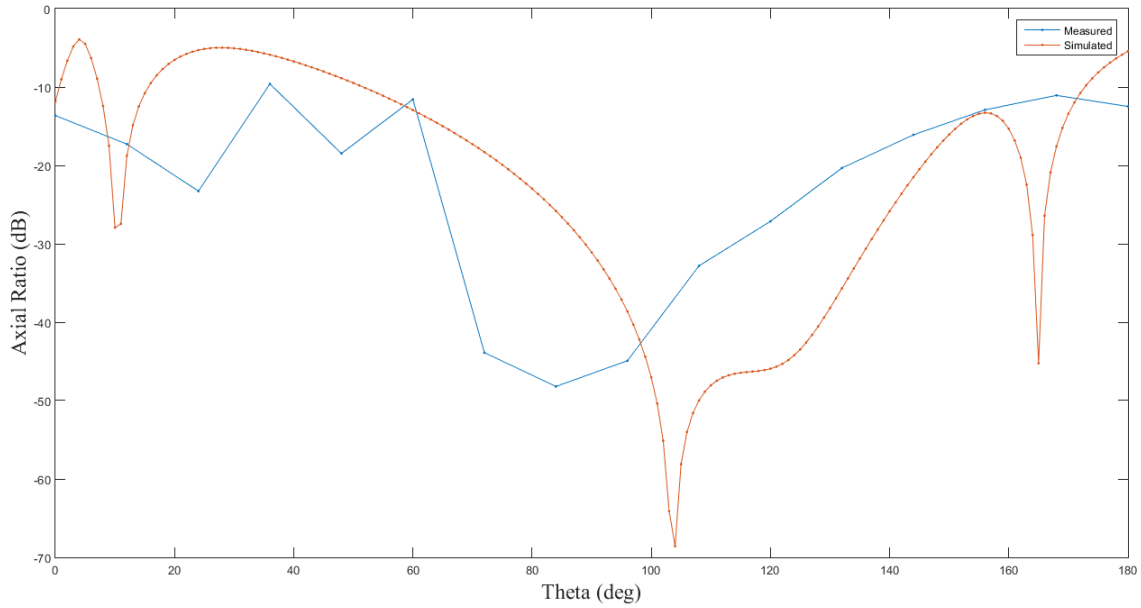

Figure 5.25: Measured *vs* Simulated axial ratio for 2.3GHz

It is possible to verify that the axial ratio presents some variations when compared to the measured and simulated values, however, these differences are not significant since they occur when the axial ratio has an already high value, which means that it is in a zone where the array works in a highly linear zone. That said, it turns out that the array is not imposing a circular polarization, so this is not the cause of loss of gain.

A detailed analysis was also done on the way the antennas and the array were integrated. As previously mentioned, the power divider was designed so the feeding vias match the exact location of the antenna feed. However, when connecting the antennas to their power divider, it was found that there was a slight deviation between the location of the track and its antenna feed, which required a longer feeding wire for the port 1 antennas when compared to that used in port 2. In addition, the wire passes close to the ground of the PCB, creating a highly capacitive effect between the ground and the signal that would go to the antenna or would come from the same, which causes the power not to be directed to the antenna, drastically reducing the gain of the array. Furthermore, due to the manufacturing process there is a slight deviation from the feed of the antenna causes the antenna not to be equal to the simulation and, in addition, it becomes unbalanced, also creating an efficiency problem.

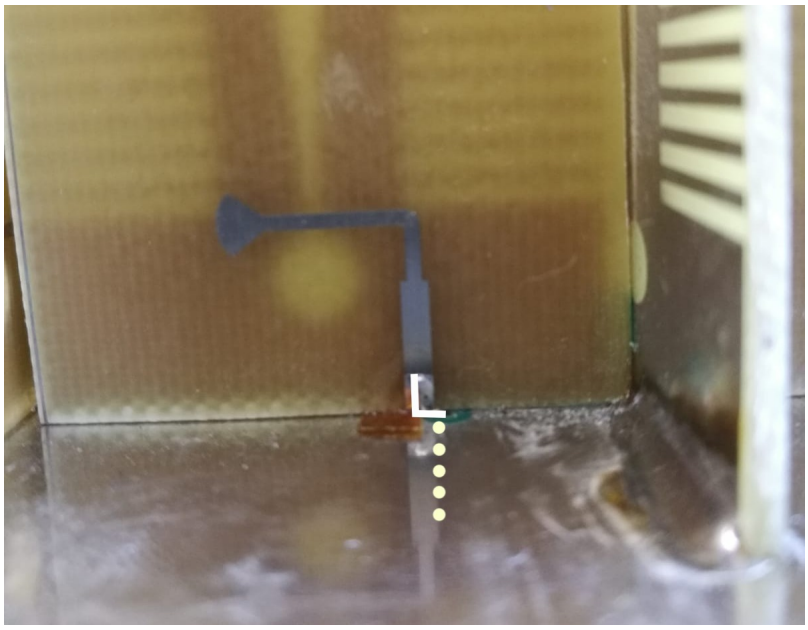

Figure 5.26: Defect of the connection between the antenna feed and the PCB

A final effect detected and to be mentioned again is that the radiation patterns for port 1 are not radiated exactly forward. A deviation of the propagation radiation can be caused by the phase of each of the feed points for this port being different from each other. In order to have a phase difference caused by the wire connecting the PCB to the antenna, there should be a difference in the length of these wires from one-tenth of the wavelength to the operating frequency of 2.3 GHz, ie about 1.3 cm apart. This does not happen since this care was taken when constructing the array. Since there were also differences between the measured and simulated values for the S-Parameters of port 1 of the array, there is the possibility of a defect in the construction of this power divider, which causes such differences in the values obtained with the simulated ones.

Chapter 6

Final remarks

6.1 Difficulties encountered

Some setbacks occurred during the development of this thesis, with emphasis for two particular situations. There were a lot of simulations to do initially to tune the antenna, which consumed a lot of computational memory, making the simulations quite slow. In order to overcome this problem, several networked computers were used in order to solve different parametric equations in different computers, thus converging more quickly to a solution that meets the requirements of the system. The other relevant situation that must be mentioned is the fact that there were not adequate equipment available to cut the antennas. In this way, all the antennas were cut by hand, subjected to a greater error, also making it difficult to replicate the system as it was simulated, leading to the possible existence of variations in the simulated parameters against the real ones. Other difficulties were related to the conjugation of the delay of the arrival of the FR4 substrate of 0.8 mm thickness due to bureaucratic problems, and the difficulty of the construction of the metamaterial by the faculty's workshop with the same substrate. As such, the finishing of the metamaterial was affected, being this factor also one of those that led to a small variation between the simulated and the real values.

6.2 Conclusions

Building a 32 Vivaldi antenna array with a metamaterial serving as polarizer is not a trivial problem. Take into account the coupling factor between antennas, isolation between feeding networks and tune the entire system to the desired frequency, make this problem highly challenging. After the study here developed, it was possible to have a developed concept to an array of antennas capable to be used in RADAR and SAR applications, although still with restrictions. It is able to be integrated into platforms such as airplanes and UAVs, being a compact and small structure. Tests already carried out prove that it is not possible to efficiently use SARs using cross-polarized antennas for emission and reception simultaneously. As such, this array of antennas with a linear wave polarizer for circular waves is intended to be an innovation in all RADAR systems and SAR

as it allows the integration of cross-polarized elements with a low coupling factor between them and capable of working simultaneously.

Throughout this dissertation, a detailed study is presented of the type of antennas used as well as the dimensions that they would have to have to fulfill the desired requirement. In addition, the way in which the array was constructed is presented and justified, always with a view to miniaturizing the system as a whole. The feeding network of the 32 antennas was also designed and simulated, presenting the problems that can arise from the construction of a multilayer PCB where it is necessary to pay close attention to the impedance of the lines so that the system continues to be adapted. In this work a dual-band polarizer is proposed that transforms a linearly polarized wave into a circularly polarized one, allowing the system to use cross-polarized Vivaldi antennas to transmit and receive signals simultaneously.

After all the simulations were completed, one started the array assembly, integrating the all the antennas as simulated and, after that, it was integrated with its feeding network. In addition, to be able to prepare the array for future SAR tests, a metal box has been built to isolate the entire array from the remaining medium, ensuring that the array will have the same behavior regardless of where the array is placed.

After the assembly of all the parts, in order to study the behavior of the system, the anechoic chamber available in faculty was used. The use of this facility allowed to characterize the array in its most varied configurations. The results show that the gain is about 10 dBi lower than the simulated one, reason why it was conducted and presented an investigation that justifies the loss of gain.

Although the results are not desired, this dissertation proves that, once the gain problem is solved, it is possible to construct a small array, compact and ready to be integrated in the most diverse RADAR and SAR support platforms, as a viable alternative to systems that use two spaced sets of antennas for signals transmission and reception.

6.3 Future work

SAR systems are increasingly being used and are at the forefront of remote sensing systems enabling the user to obtain high resolution RADAR images from a wide area regardless of weather conditions. This contribution is intended to be an important step towards the complete miniaturization of systems without loss of efficiency.

In order for this system to be totally reliable and usable without compromising good data quality, it is important to tune the frequency of operation of the metamaterial to a slightly lower frequency that continues to be covered by the array. In this way it is possible to avoid the 2.4GHz frequency which is widely used and, as such, is noisy for the system. An interesting solution to be applied also involves constructing the metamaterial using a material with fewer losses, as is the case of ceramic substrates.

Since the feeding network of port 1 of the system may be one of the problems of the system gain, it is important to reassemble the system this time on a different PCB with the same design, in order to verify that the problem actually comes from the board.

A further analysis of the behavior of the system should also be carried out to see if the gain is also reduced when compared to the simulation or if the gain already reaches an expected value. From this analysis, it can be discovered where this lack of system power comes from which is leading to loss of gain at operating frequency of 2.3 GHz.

After the system was fully tuned and, a full SAR test using an airplane must be conducted in order to fully validate the system under the environmental conditions to which it will be subject.

Bibliography

[1] Joash P Rodriguez, Kevin M Martin, and Miguel Carlo L Purisima. Design and implementation of a continuously steerable antenna array for synthetic aperture radar applications. In *Antenna Measurements & Applications (CAMA), 2015 IEEE Conference on*, pages 1–4. IEEE, 2015.

[2] Microsoft powerpoint - ltc2013-sar-moreira-v5.pptx. https://earth.esa.int/documents/10174/642943/6-LTC2013-SAR-Moreira.pdf.

[3] Constantine A Balanis. *Modern antenna handbook*. John Wiley & Sons, 2011.

[4] David M Pozar. *Microwave engineering*. John Wiley & Sons, 2009.

[5] How and why to use pin diodes for rf switching | digikey. https://www.digikey.com/en/articles/techzone/2016/dec/how-and-why-to-use-pin-diodes-for-rf-switching.

[6] Sen Yan. Metamaterial design and its application for antennas. 2015.

[7] Naobumi Michishita. Expectation for metamaterials for antenna applications. In *Antennas and Propagation (ISAP), 2016 International Symposium on*, pages 558–559. IEEE, 2016.

[8] A. Moreira, P. Prats-Iraola, M. Younis, G. Krieger, I. Hajnsek, and K. P. Papathanassiou. A tutorial on synthetic aperture radar. *IEEE Geoscience and Remote Sensing Magazine*, 1(1):6–43, March 2013. doi:10.1109/MGRS.2013.2248301.

[9] Lecture 4: Synthetic aperture radar (sar). https://ocw.mit.edu/resources/res-ll-003-build-a-small-radar-system-capable-of-sensing-range-doppler-and-lecture-notes/MITRES_LL_003IAP11_lec04.pdf.

[10] PJ Gibson. The vivaldi aerial. In *Microwave Conference, 1979. 9th European*, pages 101–105. IEEE, 1979.

[11] Yakup Erdogan. Parametric study and design of vivaldi antennas and arrays. *Middle East Technical University, Ankara, Turkey*, 2009.

[12] Gaurav Kumar Pandey and Manoj Kumar Meshram. A printed high gain uwb vivaldi antenna design using tapered corrugation and grating elements. *International Journal of RF and Microwave Computer-Aided Engineering*, 25(7):610–618, 2015.

[13] C.A. Balanis. *Antenna Theory: Analysis and Design*. Number vol. 1 in Antenna Theory: Analysis and Design. John Wiley & Sons, 2005.

[14] Eko Setijadi, Gamantyo Hendrantoro, et al. Effect of vivaldi element pattern on the uniform linear array pattern. In *Communication, Networks and Satellite (COMNETSAT), 2016 IEEE International Conference on*, pages 42–47. IEEE, 2016.

[15] Ieee standard for definitions of terms for antennas. *IEEE Std 145-2013 (Revision of IEEE Std 145-1993)*, pages 1–50, March 2014. doi:10.1109/IEEESTD.2014.6758443.

[16] Koichiro Takamizawa. *Analysis of highly coupled wideband antenna arrays using scattering parameter network models*. PhD thesis, Virginia Tech, 2002.

[17] M. Lapine and S. Tretyakov. Contemporary notes on metamaterials. *IET Microwaves, Antennas Propagation*, 1(1):3–11, February 2007. doi:10.1049/iet-map:20050307.

[18] Pankaj Kumar, Zubair Akhter, Abhishek Kr Jha, and M Jaleel Akhtar. Directivity enhancement of double slot vivaldi antenna using anisotropic zero-index metamaterials. In *Antennas and Propagation & USNC/URSI National Radio Science Meeting, 2015 IEEE International Symposium on*, pages 2333–2334. IEEE, 2015.

[19] Ansys electronics desktop: Electromagnetic analysis. https://www.ansys.com/products/electronics/ansys-electronics-desktop.

[20] Advanced design system (ads) | keysight (formerly agilent's electronic measurement). https://www.keysight.com/en/pc-1297113/advanced-design-system-ads?cc=PT&lc=eng.

[21] Yongzhi Cheng, Yan Nie, Zhengze Cheng, and Rong Zhou Gong. Dual-band circular polarizer and linear polarization transformer based on twisted split-ring structure asymmetric chiral metamaterial. *Progress In Electromagnetics Research*, 145:263–272, 2014.

[22] Electromagnetic simulation software | altair feko. https://altairhyperworks.com/product/FEKO. (Accessed on 05/10/2018).